Title: Secreted Amyloid-β Precursor Protein Functions as a GABA$_B$R1a Ligand to Modulate Synaptic Transmission

Authors: Heather C. Rice[1,2], Daniel de Malmazet[3,4], An Schreurs[5], Samuel Frere[6], Inge Van Molle[7], Alexander N. Volkov[7,8], Eline Creemers[1,2], Irena Vertkin[6], Julie Nys[1,2], Fanomezana M. Ranaivoson[9,10], Davide Comoletti[9,11], Jeffrey N. Savas[12], Han Remaut[7], Detlef Balschun[5], Keimpe D. Wierda[1,2], Inna Slutsky[6], Karl Farrow[3,4,13,14], Bart De Strooper[1,2,15,*], and Joris de Wit[1,2,*]

Affiliations:

[1] VIB Center for Brain & Disease Research, Leuven, Belgium

[2] KU Leuven, Department of Neurosciences, Leuven Brain Institute, Leuven, Belgium

[3] Neuro-Electronics Research Flanders, Leuven, Belgium

[4] KU Leuven, Department of Biology, Leuven Brain Institute, Leuven, Belgium

[5] KU Leuven, Brain & Cognition, Leuven, Belgium

[6] Department of Physiology and Pharmacology, Sackler Faculty of Medicine and Sagol School of Neuroscience, Tel Aviv University, Tel Aviv, Israel

[7] VIB-VUB Structural Biology Research Center, Brussels, Belgium

[8] Jean Jeener NMR Centre, VUB, Brussels, Belgium

[9] Child Health Institute of New Jersey and Department of Neuroscience and Cell Biology, Robert Wood Johnson Medical School, Rutgers University, New Brunswick, New Jersey, USA

[10] Present Address: Structural Motility, Institut Curie, PSL Research University, CNRS, UMR 144, Paris, France

[11] Present Address: School of Biological Sciences, Victoria University of Wellington, Wellington, New Zealand

[12] Department of Neurology, Feinberg School of Medicine, Northwestern University, Chicago, IL, USA

[13] VIB, Leuven, Belgium

[14] imec, Leuven, Belgium

[15] UK-Dementia Research Institute at University College London, UK

*Correspondence to: bart.destrooper@kuleuven.vib.be; joris.dewit@kuleuven.vib.be

Abstract:

Amyloid-β precursor protein (APP) is central to the pathogenesis of Alzheimer's disease, yet its physiological function remains unresolved. Accumulating evidence suggests that APP has a synaptic function mediated by an unidentified receptor for the shed APP ectodomain (sAPP). Here, we showed that the sAPP extension domain directly bound the sushi 1 domain specific to the gamma-aminobutyric acid type B receptor subunit 1a (GABA$_B$R1a). sAPP-GABA$_B$R1a binding suppressed synaptic transmission and enhanced short-term facilitation in hippocampal synapses via inhibition of synaptic vesicle release. A 17 amino acid peptide corresponding to the GABA$_B$R1a binding region within APP suppressed spontaneous neuronal activity *in vivo*. Our findings identify GABA$_B$R1a as a synaptic receptor for sAPP and reveal a physiological role for sAPP in regulating GABA$_B$R1a function to modulate synaptic transmission.

One Sentence Summary:

Amyloid-β precursor protein suppresses vesicle release from presynaptic boutons by binding to the sushi domain of the GABA$_B$1a receptor.

Main Text:

Amyloid-β Precursor Protein (APP), a type 1 transmembrane protein, was first identified more than 30 years ago (*1–4*) as the precursor to the amyloid-β peptide, the primary constituent of amyloid plaques found in the brains of Alzheimer's disease (AD) patients. APP undergoes ectodomain shedding by α-, β-, or η- secretase to release soluble APP (sAPPα, sAPPβ, or sAPPη respectively) (*5*, *6*). Evidence suggests that the synaptic function of APP (*7–13*) is carried out by sAPP (*14*, *15*). sAPPα affects synaptic transmission and plasticity, including a reduction in synaptic activity and an enhancement of LTP (*16–19*). Moreover, sAPPα is sufficient to rescue synaptic defects in *App* KO mice, including defects in spine density (*20*), LTP (*21*, *22*), and spatial learning (*21*). Together, this has led to speculation of a yet unidentified cell-surface receptor for sAPP to mediate its synaptic function (*15*, *23*, *24*).

Proteomics screen for synaptic interactors of sAPP identifies GABA$_B$R

We first confirmed, using biochemical fractionation and structured illumination imaging, that APP was abundantly expressed at presynaptic terminals (*25*) of excitatory and inhibitory hippocampal synapses (Fig. S1A,B). Next, to identify candidate synaptic receptors for sAPP, we performed an extensive series of affinity purification experiments using recombinant sAPP-Fc (C-terminal Fc-tag; affinity purified from transfected-HEK293T supernatants; Fig. S2A,B) to pull down interacting proteins from synaptosome extracts, followed by mass spectrometric analysis of bound proteins (AP-MS) (Fig. 1A) (*26*). We consistently identified, among a few intracellular proteins (Fig 1B, S3A,B, Table S1), the gamma-aminobutyric acid type B receptor subunit 1 (GABA$_B$R1) as the most abundant and reproducible cell-surface protein, using sAPPα or sAPPβ as bait, in wildtype (WT) and in App/Aplp1 knockout (KO) synaptosome extracts (Fig. 1B, S3A,B, Table

S1). Supporting our observations, APP has previously been identified in a GABA$_B$R interactome analysis (*27*). Together, the sAPP AP-MS experiments identified GABA$_B$R as the leading candidate for a synaptic, cell-surface receptor for sAPP.

The extension domain of APP binds the sushi 1 domain of GABA$_B$R1a

GABA$_B$R, the metabotropic receptor for the inhibitory neurotransmitter GABA, regulates presynaptic neurotransmitter release and postsynaptic membrane excitability (*28*). It consists of two subunits: GABA$_B$R1 which binds GABA, and GABA$_B$R2 which couples to G proteins (*29*). Two major isoforms, GABA$_B$R1a and GABA$_B$R1b, differ by two N-terminal sushi repeats only present in the a-variant (*29*) (Fig 1C). To validate the proteomics results, we performed cell-surface binding assays, applying recombinant sAPPα-Fc to HEK293T cells expressing the GABA$_B$R ectodomain on the plasma membrane using the pDisplay vector. sAPPα-Fc, but not Fc alone, bound strongly to GABA$_B$R1a-, but not to GABA$_B$R1b-, or GABA$_B$R2-, expressing cells (Fig. 1D). Biolayer interferometry experiments using recombinant sAPPα (Fc-tag enzymatically removed; Fig. S2C-F) and GABA$_B$R1a sushi domains showed that the sushi 1 peptide was sufficient for binding sAPPα (Fig. 1E). Accordingly, excess sushi 1 peptide blocked binding of sAPPα-Fc to GABA$_B$R1a-expressing cells (Fig. 1F). Isothermal titration calorimetry (ITC) determined the dissociation constant (K_D) for sAPPα-sushi 1 = 431 nM (Fig. 1G). These data show that sAPPα binds directly and selectively to the sushi 1 domain of GABA$_B$R1a with sub-micromolar affinity.

The ectodomain of the APP695 isoform contains several functional domains (Fig. 2A). Surprisingly, growth factor like domain (GFLD)-Fc, copper binding domain (CuBD)-Fc, and E2-Fc each failed to bind GABA$_B$R1a-expressing cells (Fig. 2B). However, a peptide corresponding

to the natively unstructured linker region between the APP695 E1 and E2 domains (Fig. 2A) strongly binds to GABA$_B$R1a-expressing cells (Fig. 2B). The linker region includes the acidic domain (AcD) and the recently defined extension domain (ExD), which is a flexible, partially structured region (*30*). The binding affinity of the purified ExD-AcD fragment (Fc-tag enzymatically removed) to sushi 1 in ITC experiments (Fig. 2C) was in the same range as that of full-length sAPPα binding to sushi 1 (Fig. 1G). To further narrow down the minimal domain in the APP linker region required for sushi 1 binding, we generated ExD-Fc and AcD-Fc fragments. ExD-Fc, but not AcD-Fc, bound to GABA$_B$R1a-expressing cells (Fig. 2B), identifying the ExD as the minimal domain required for sushi 1 binding. Consequently, deletion of the ExD in sAPPα (sAPPαΔExD-Fc) abolished binding to GABA$_B$R1a-expressing cells (Fig. 2B). sAPPβ-Fc and sAPPη-Fc, a product of the recently described η-secretase processing pathway (*6*), which both contain the ExD, also bound to GABA$_B$R1a-expressing cells (Fig 2D). APP family members APP-like protein 1 and 2 (APLP1 and APLP2) (*31*) on the other hand lack a conserved ExD and failed to bind GABA$_B$R1a-expressing cells (Fig. 2E). Thus, the sAPP ExD is necessary and sufficient to bind to the GABA$_B$R1a sushi 1 domain.

sAPP suppresses presynaptic vesicle release probability via GABA$_B$R1a

Sushi domain-containing GABA$_B$R1a is the predominant isoform localized to presynaptic compartments at excitatory synapses (*32–34*), where it functions to inhibit neurotransmitter release (*28*). To test whether sAPPα can modulate GABA$_B$R function, we simultaneously measured miniature excitatory and inhibitory postsynaptic currents (mEPSCs and mIPSCs), which were separated on the basis of their distinct decay kinetics as described (*35*), in cultured mouse hippocampal neurons (12-17 days in vitro (DIV)) (Fig. 3A). Consistent with previous observations

(*36*, *37*), acute exposure of hippocampal neurons to 30 μM baclofen, a GABA$_B$R agonist, reduced the frequency of mEPSCs by 63 ± 5% (n=14 cells; P < 0.001) (Fig. S4A,B). Likewise, 250 nM sAPPα (Fc-tag removed) reduced the frequency of mEPSCs by 39 ± 5% (n=13 cells; P < 0.001) (Fig. 3B,C), an effect that was already apparent at 25nM (Fig. S4D,E), without affecting mEPSC amplitude (Fig. S4C). sAPPβ similarly reduced mEPSC frequency (Fig. S4D,E). Acute application of the APP695 ExD-AcD fragment reduced mEPSC frequency to a similar degree as sAPPα (Fig. 3D, S4F), whereas application of sAPPαΔExD had no effect (Fig. 3D, S4F), indicating that the extension domain of sAPP is necessary and sufficient for the suppression of spontaneous glutamatergic synaptic transmission by sAPPα. Accordingly, acute application of sAPLP1, which lacks a conserved ExD, did not reduce mEPSC frequency (Fig. S4G), although we observed a minor (17 ± 9 %; n=17 cells; P < 0.05) reduction in mIPSC frequency (Fig. S4H). Pretreatment with the GABA$_B$R antagonist CGP55845 (CGP, 5 μM) attenuated the sAPPα-mediated reduction of mEPSC frequency (Fig. 3E, S4I), showing that the effect is mediated by GABA$_B$R.

GABA$_B$R1a also localizes to GABAergic boutons (*34*). Consistent with previous observations (*37*, *38*), acute exposure of hippocampal neurons to 30 μM baclofen reduced the frequency of mIPSCs by 62 ± 5% (n=14 cells; P < 0.001) (Fig. S5A). Acute application of 250 nM sAPPα to hippocampal neurons reduced the frequency of mIPSCs by 44 ± 5% (n=13 cells; P < 0.001) (Fig. 3B, S5B). Application of sAPPα caused a minor (14%) reduction in mIPSC amplitude (Fig. S5C), possibly due to a small post-synaptic effect of sAPPα on GABA$_B$R1a at post-synaptic GABAergic sites (*39*). The APP695 ExD-AcD fragment, but not sAPPαΔExD, reduced mIPSC frequency to a similar extent as sAPPα (Fig. S4F, S5D). The effect of sAPPα on mIPSC frequency was blocked by pretreatment with the GABA$_B$R antagonist CGP55845 (CGP, 5 μM) (Fig. S4I, S5E). Taken

together, these data show that sAPPα acutely reduces both glutamatergic and GABAergic quantal synaptic transmission through a GABA$_B$R1a isoform-dependent mechanism.

sAPPα might exert its effect on synaptic transmission by interfering with a complex of full-length APP and GABA$_B$R1a. In neurons lacking APP however, sAPPα still reduced mEPSC and mIPSC frequency (Fig. S6A,B), excluding this possibility. Application of 30 µM baclofen similarly reduced mEPSC and mIPSC frequency in *App*/*Aplp1* dKO cultures (Fig. S6C,D) as in WT cultures (Fig. 3C, S5B), suggesting that the absence of full-length APP does not cause major alterations in GABA$_B$R localization to presynaptic terminals. However, the possibility that full-length APP also interacts with and affects GABA$_B$R signaling separate from the effects of sAPPα reported here cannot be excluded.

The decrease in mEPSC frequency but not amplitude following acute sAPPα application suggests a change in presynaptic release properties. We therefore assessed the effect of sAPPα on presynaptic vesicle recycling using the fluorescent membrane dye FM1-43. We measured presynaptic strength by measuring the density (D) of FM+ boutons per image area and the change in fluorescence intensity (ΔF) of FM1-43 signals at individual boutons of cultured hippocampal neurons using a combined FM1-43 loading/unloading stimulation paradigm (Fig. 3F). Application of sAPPα decreased the total presynaptic strength ($S = \Delta F \times D$) across synaptic populations (Fig. 3G, S7A) in a dose-dependent manner (Fig. 3H), reaching 57 ± 7 % (n=8 experiments; $P < 0.001$) reduction at 1 µM sAPPα. This decrease was not observed with deletion of the ExD (sAPPαΔExD, 1 µM) (Fig. 3H, S7B) and was occluded by the GABA$_B$R antagonist CGP54626 (CGP, 10µM) (Fig 3I, S7C), indicating that GABA$_B$R1a mediates the presynaptic inhibition induced by sAPPα.

sAPP enhances short-term plasticity at Schaffer collateral synapses in a GABA$_B$R1a-dependent manner

We next assessed the effect of sAPPα on synaptic transmission in an intact circuit at CA3-CA1 Schaffer collateral (SC) synapses, which exclusively contain GABA$_B$R1a receptors (*32*). We measured field EPSPs (fEPSPs) evoked by low frequency stimulation (0.1 Hz) at varying intensities (30-150 μA) in CA1 stratum radiatum after 90 min pre-incubation of acute hippocampal slices with or without 1 μM sAPPα (Fig 4A). Treatment with sAPPα reduced fEPSP amplitude and decreased the slope of the input/output (i/o) curve by 23% (Fig. S8A), indicating that sAPPα suppresses basal synaptic transmission at SC synapses. To specifically assess if sAPPα affects presynaptic properties, we applied a burst of 5 stimuli at 3 different frequencies (20, 50, and 100 Hz) to induce short-term facilitation, which inversely correlates with the probability of neurotransmitter release. Facilitation was higher for each frequency tested in sAPPα-incubated compared to control slices (Fig. 4B, S8B,C). Analysis of the paired-pulse ratio (PPR) for the first 2 stimuli showed an increased PPR for each frequency following sAPPα treatment (Fig. 4C), indicating a decreased release probability. Deletion of the ExD (sAPPαΔExD 1 μM) abolished the sAPPα-mediated effect on the i/o curve (Fig. S9D), short-term facilitation (Fig. 4D, S8E,F), and PPR (Fig. 4E). In addition, preincubation of slices with the GABA$_B$R antagonist CGP54626 (CGP, 10 μM) abolished the sAPPα-mediated decrease in the slope of the i/o curve (Fig. S8G) and occluded the sAPPα-induced increase in short-term facilitation and PPR at each frequency (Fig. 4F,G, S8H,I), demonstrating GABA$_B$R-dependence of these effects. Altogether, these results indicate that sAPPα controls vesicle release at SC synapses by acting on presynaptic GABA$_B$R1a.

A short peptide within the APP ExD suppresses synaptic vesicle release via GABA$_B$R1a

A GABA$_B$R1a isoform-specific modulator has potential therapeutic implications for a number of neurological disorders involving GABA$_B$R signaling (*29*). Since we observed that purified protein corresponding to the linker region of APP (Fig. 2A) was sufficient to mimic the effects of sAPPα on mEPSC frequency (Fig. 3D), we set out to identify the minimally active region within the ExD. Alignment of the sAPP ExD (amino acids (AA) 195-227 of APP695) from seven vertebrate species revealed the strongest conservation within a 17AA stretch (204-220AA; Fig. 5A). The corresponding synthetic APP 17mer peptide bound sushi 1 of GABA$_B$R1a with a K_D of 810nM (Fig. 5B), in the same range as the binding affinity of the entire linker region (Fig. 2C). Shortening the peptide to a synthetic 9mer consisting of APP695 residues 204-212 (APP 9mer) lowered the K_D to 2.3 μM (Fig. 5C); whereas residues 211-220 failed to bind sushi 1 (Fig. S9A). Thus, a conserved, minimal 9AA sequence within the sAPP ExD is sufficient for direct binding to the sushi 1 domain of GABA$_B$R1a.

To gain further insight in the binding of the APP 9mer to the GABA$_B$R1a sushi 1 domain, we used nuclear magnetic resonance (NMR) spectroscopy. As previously reported (*40*), we observed that the sushi 1 domain of GABA$_B$R1a is natively unstructured (Fig. S9B). Strikingly, APP 9mer binding stabilized the sushi 1 domain of GABA$_B$R1a, allowing determination of its solution structure (Figure 5D, S9C) and generation of a structural model of the complex (Fig. 5E). In our model, a valine and tryptophan at 208-209AA of APP695 bind within a pocket of sushi 1, formed by the loops and the short beta-strand in the N-terminal part of the protein (32-53 AA of full-length GABA$_B$R1a) (Fig. S9D). Thus, APP binding induces a conformational change in the natively unstructured sushi 1 domain of GABA$_B$R1a. This structure-function relationship strongly supports the physiological relevance of the interaction.

As the affinity for sushi 1 was better retained in the APP 17mer compared to the 9mer (Fig. 5B,C), we next tested whether the APP 17mer could functionally mimic sAPPα. Acute application of the APP 17mer peptide, but not of a scrambled 17mer control peptide, reduced mEPSC frequency in hippocampal neurons to a similar degree as sAPPα (Fig. 5F, S9E) and was already apparent at 25 nM (Fig. S9F). Pretreatment with the GABA$_B$R antagonist CGP55845 (CGP, 5µM) blocks this effect (Fig. 5G, S9G). Together, these findings show that the APP 17mer peptide mimics the effects of sAPPα on GABA$_B$R1a-dependent inhibition of synaptic vesicle release.

APP 17mer peptide suppresses neuronal activity of CA1 pyramidal cells *in vivo*

In the final series of experiments, we utilized the APP 17mer peptide as a tool to examine the effects of sAPP-GABA$_B$R signaling on neuronal activity *in vivo*. Using two-photon calcium imaging, we measured calcium transients of CA1 hippocampal neurons in anesthetized Thy1-GCaMP6s mice before (baseline) and after a 60-90 min superfusion of the exposed hippocampus with either baclofen (30 µM), APP 17mer (5µM), or scrambled 17mer control peptide (5µM) (Fig. 6A). Application of 30 µM baclofen caused a dramatic decrease in the frequency of calcium transients compared to baseline (Fig. S10A-C), indicating that activation of GABA$_B$Rs strongly suppresses neuronal activity in CA1 pyramidal neurons *in vivo*. Consistent with our results in cultured hippocampal neurons, application of the APP 17mer significantly reduced the frequency of calcium transients compared to baseline (Fig. 6B-D, Movie S1). The frequency of calcium transients was restored back to baseline following a two-hour wash-out of the peptide (Fig. S10D-F), indicating that the suppression of CA1 neuron activity by the APP 17mer peptide is reversible. Furthermore, the scrambled 17mer control peptide did not affect the frequency of calcium

transients (Fig. 6E-G; S10G-I, Movie S2). Together, these results indicate that APP inhibits neuronal activity *in vivo* and that the GABA$_B$R1a binding domain is sufficient for such inhibition.

Discussion

Our studies reveal that sAPP acts as a GABA$_B$R1a-specific ligand to suppress synaptic vesicle release. Consequently, sAPP modulates hippocampal synaptic plasticity and neurotransmission *in vivo*. APP is among the most abundant proteins in synaptic boutons (*25*), and deletion of *App* in mice leads to synaptic deficits (*7–9*, *21*, *22*). Synaptic activity enhances proteolytic processing of APP (*41*, *42*) and GABA$_B$R is a key regulator of homeostatic synaptic plasticity (*43*). Hence, our observations raise the possibility that the sAPP-GABA$_B$R1a interaction acts as an activity-dependent negative feedback mechanism to suppress synaptic release and maintain proper homeostatic control of neural circuits. While AD-causing mutations in APP all affect Aβ generation, it is not entirely clear whether other aspects of APP function contribute to AD. Network abnormalities such as hyperexcitability and hypersynchronization precede clinical onset of AD in human patients (*44*). Some studies indicate that sAPP levels may be altered in AD (*14*). Interestingly, a GABA$_B$R antagonist has been shown to improve memory in animal models and patients with mild cognitive impairment (*45–47*). Moreover, as most transgenic AD mouse models overexpress sAPP, the role of sAPP in synaptic phenotypes of transgenic APP mice should be considered, particularly given evidence that network hyperexcitability in these mice is independent of Aβ production (*48*).

GABA$_B$R signaling has been implicated in a number of neurological and psychiatric disorders including epilepsy, depression, addiction, and schizophrenia (*49*). Selective binding partners of the GABA$_B$R1a sushi domains are of potential therapeutic interest due to localization and functional

differences of GABA$_B$R1 isoforms (*32*, *50*) as well as the adverse effects of current non-specific agonists (*29*). The identification of sAPP as a functional GABA$_B$R1a-specific binding partner provides a target for the development of therapeutic strategies for modulating GABA$_B$R1a-specific signaling in neurological and psychiatric disorders. The identification of short APP peptides that confer structure in the GABA$_B$R1a sushi 1 domain and modulate neurotransmission *in vivo* are major steps towards development of a GABA$_B$R1a isoform-specific therapeutic.

Summary of Methods

To identify candidate synaptic interactors for sAPP, affinity purification experiments were performed using recombinant sAPP-Fc to pull down interacting proteins from synaptosome extracts, followed by mass spectrometric analysis of bound proteins. Cell surface binding assays, biolayer interferometry, and isothermal titration calorimetry were used to determine domains of interaction and apparent binding affinities between sAPP to GABA$_B$R. Nuclear magnetic resonance spectroscopy was used to generate a structural model of the APP-GABA$_B$R complex. The function of the sAPP-GABA$_B$R interaction was investigated by accessing spontaneous postsynaptic currents and FM1-43 dye labeling in mouse hippocampal cultures, short-term facilitation in acute hippocampal slices, and 2-photon *in vivo* calcium imaging in CA1 hippocampus of anesthetized Thy1-GCaMP6 mice. The details of each of these methods are described in the supplementary materials.

References and Notes:

1. D. Goldgaber, M. Lerman, O. W. McBride, U. Saffiotti, D. C. Gajdusek, Characterization and Chromosomal Localization of a cDNA Encoding Brain Amyloid of Alzheimer's Disease. *Science*. **235**, 877–880 (1987).

2. N. K. Robakis, N. Ramakrishna, G. Wolfe, H. M. Wisniewski, Molecular Cloning and Characterization of a cDNA Encoding the Cerebrovascular and the Neuritic Plaque Amyloid Peptides. *Proc. Natl. Acad. Sci.* **84**, 4190–4194 (1987).

3. N. R. Tanzi RE, Gusella JF, Watkins PC, Bruns GA, St George-Hyslop P, Van Keuren ML, Patterson D, Pagan S, Kurnit DM, Amyloid beta protein gene: cDNA, mRNA distribution, and genetic linkage near the Alzheimer locus. *Science*. **235** (1987).

4. J. Kang *et al.*, The precursor of Alzheimer's disease amyloid A4 protein resembles a cell-surface receptor. *Nature*. **325** (1987), pp. 733–6.

5. C. Haass, C. Kaether, G. Thinakaran, S. Sisodia, Trafficking and proteolytic processing of APP. *Cold Spring Harb. Perspect. Med.* **2** (2012), doi:10.1101/cshperspect.a006270.

6. M. Willem *et al.*, η-Secretase processing of APP inhibits neuronal activity in the hippocampus. *Nature*. **526**, 443–447 (2015).

7. G. R. Dawson *et al.*, Age-related cognitive deficits, impaired long-term potentiation and reduction in synpatic marker density in mice lacking the beta-amyloid precursor protein. *Neuroscience*. **90**, 1–13 (1999).

8. G. R. Seabrook *et al.*, Mechanisms contributing to the deficits in hippocampal synaptic plasticity in mice lacking amyloid precursor protein. *Neuropharmacology*. **38**, 349–359 (1999).

9. S.-H. Tyan *et al.*, Amyloid precursor protein (APP) regulates synaptic structure and function. *Mol. Cell. Neurosci.* **51**, 43–52 (2012).

10. S. M. Fitzjohn *et al.*, Similar levels of long-term potentiation in amyloid precursor protein - null and wild-type mice in the CA1 region of picrotoxin treated slices. *Neurosci. Lett.* **288**, 9–12 (2000).

11. L. Yang, Z. Wang, B. Wang, N. J. Justice, H. Zheng, Amyloid Precursor Protein Regulates Ca v 1 . 2 L-type Calcium Channel Levels and Function to Influence GABAergic Short-Term Plasticity. *Neuroscience*. **29**, 15660–15668 (2009).

12. B. Wang *et al.*, The Amyloid Precursor Protein Controls Adult Hippocampal Neurogenesis through GABAergic Interneurons. *J Neurosci*. **34**, 13314–13325 (2014).

13. M. Chen, J. Wang, J. Jiang, X. Zheng, N. J. Justice, APP modulates KCC2 expression and function in hippocampal GABAergic inhibition, 1–26 (2017).

14. B. G. Mockett, M. Richter, W. C. Abraham, U. C. Müller, Therapeutic Potential of Secreted Amyloid Precursor Protein APPsα. *Front. Mol. Neurosci.* **10**, 30 (2017).

15. U. C. Müller, T. Deller, M. Korte, Not just amyloid : physiological functions of the amyloid precursor protein family. *Nat. Rev. Neurosci.* (2017), doi:10.1038/nrn.2017.29.

16. K. Furukawa, S. W. Barger, E. M. Blalock, M. P. Mattson, Activation of K+ channels and suppression of neuronal activity by secreted beta-amyloid-precursor protein. *Nature*. **379** (1996), pp. 74–78.

17. A. Ishida, K. Furukawa, J. N. Keller, M. P. Mattson, Secreted form of beta-amyloid precursor protein shifts the frequency dependency for induction of LTD, and enhances LTP in hippocampal slices. *Neuroreport*. **8**, 2133–7 (1997).

18. C. J. Taylor *et al.*, Endogenous secreted amyloid precursor protein-α regulates hippocampal NMDA receptor function, long-term potentiation and spatial memory. *Neurobiol. Dis.* **31**, 250–260 (2008).

19. M. Xiong *et al.*, Secreted amyloid precursor protein-alpha can restore novel object location memory and hippocampal LTP in aged rats. *Neurobiol. Learn. Mem.* **138**, 291–299 (2017).

20. S. W. Weyer *et al.*, Comparative analysis of single and combined APP/APLP knockouts reveals reduced spine density in APP-KO mice that is prevented by APPsα expression. *Acta Neuropathol. Commun.* **2**, 36 (2014).

21. S. Ring *et al.*, The secreted beta-amyloid precursor protein ectodomain APPs alpha is sufficient to rescue the anatomical, behavioral, and electrophysiological abnormalities of APP-deficient mice. *J. Neurosci.* **27**, 7817–7826 (2007).

22. M. Hick *et al.*, Acute function of secreted amyloid precursor protein fragment APPsα in synaptic plasticity. *Acta Neuropathol.* **129**, 21–37 (2015).

23. T. Saitoh *et al.*, Secreted form of amyloid-beta protein precursor is involved in the growth regulation of fibroblasts. *Cell*. **58**, 615–622 (1989).

24. C. Reinhard, M. Borgers, G. David, B. De Strooper, Soluble amyloid-β precursor protein binds its cell surface receptor in a cooperative fashion with glypican and syndecan proteoglycans. *J. Cell Sci.* **126**, 4856–61 (2013).

25. B. G. Wilhelm *et al.*, Composition of isolated synaptic boutons reveals the amounts of vesicle trafficking proteins. *Science*. **344**, 1023–8 (2014).

26. J. N. Savas *et al.*, Ecto-Fc MS identifies ligand-receptor interactions through extracellular domain Fc fusion protein baits and shotgun proteomic analysis. *Nat. Protoc.* **9**, 2061–2074 (2014).

27. J. Schwenk *et al.*, Modular composition and dynamics of native GABAB receptors identified by high-resolution proteomics. *Nat. Neurosci.* **19** (2015), doi:10.1038/nn.4198.

28. M. Gassmann, B. Bettler, Regulation of neuronal GABAB receptor functions by subunit composition. *Nat. Rev. Neurosci.* **13**, 380–394 (2012).

29. J.-P. Pin, B. Bettler, Organization and functions of mGlu and GABAB receptor complexes. *Nature*. **540**, 60–68 (2016).

30. I. Coburger *et al.*, Analysis of the overall structure of the multi-domain amyloid precursor protein (APP). *PLoS One*. **8**, 1–12 (2013).

31. S. A. M. Shariati, B. De Strooper, Redundancy and divergence in the amyloid precursor protein

family. *FEBS Lett.* **587**, 2036–2045 (2013).

32. R. Vigot *et al.*, Differential Compartmentalization and Distinct Functions of GABAB Receptor Variants. *Neuron*. **50**, 589–601 (2006).

33. B. Biermann *et al.*, The Sushi domains of GABAB receptors function as axonal targeting signals. *J. Neurosci.* **30**, 1385–94 (2010).

34. P. C. Waldmeier, K. Kaupmann, S. Urwyler, Roles of GABAB receptor subtypes in presynaptic auto- and heteroreceptor function regulating GABA and glutamate release. *J. Neural Transm.* **115**, 1401–1411 (2008).

35. K. D. B. Wierda, J. B. Sørensen, Innervation by a GABAergic neuron depresses spontaneous release in glutamatergic neurons and unveils the clamping phenotype of synaptotagmin-1. *J. Neurosci.* **34**, 2100–10 (2014).

36. M. Scanziani, M. Capogna, B. H. Gähwiler, S. M. Thompson, Presynaptic inhibition of miniature excitatory synaptic currents by baclofen and adenosine in the hippocampus. *Neuron*. **9**, 919–927 (1992).

37. M. Iyadomi, I. Iyadomi, E. Kumamoto, K. Tomokuni, M. Yoshimura, Presynaptic inhibition by baclofen of miniature EPSCs and IPSCs in substantia gelatinosa neurons of the adult rat spinal dorsal horn. *Pain*. **85**, 385–393 (2000).

38. J. Rohrbacher, W. Jarolimek, a Lewen, U. Misgeld, GABAB receptor-mediated inhibition of spontaneous inhibitory synaptic currents in rat midbrain culture. *J. Physiol.* **500 (Pt 3**, 739–49 (1997).

39. D. Ulrich, B. Bettler, GABAB receptors: synaptic functions and mechanisms of diversity. *Curr. Opin. Neurobiol.* **17**, 298–303 (2007).

40. S. Blein *et al.*, Structural analysis of the complement control protein (CCP) modules of GABAB receptor 1a: Only one of the two CCP modules is compactly folded. *J. Biol. Chem.* **279**, 48292–48306 (2004).

41. R. M. Nitsch, S. a Farber, J. H. Growdon, R. J. Wurtman, Release of amyloid beta-protein precursor derivatives by electrical depolarization of rat hippocampal slices. *Proc. Natl. Acad. Sci. U. S. A.* **90**, 5191–5193 (1993).

42. F. Kamenetz *et al.*, APP Processing and Synaptic Function. *Neuron*. **37**, 925–937 (2003).

43. I. Vertkin *et al.*, GABAB receptor deficiency causes failure of neuronal homeostasis in hippocampal networks. *Proc. Natl. Acad. Sci. U. S. A.* **112**, E3291-3299 (2015).

44. J. J. Palop, L. Mucke, Network abnormalities and interneuron dysfunction in Alzheimer disease. *Nat. Rev. Neurosci.* **17**, 777–792 (2016).

45. Y. Li *et al.*, Implications of GABAergic Neurotransmission in Alzheimer's Disease. *Front. Aging Neurosci.* **8**, 1–12 (2016).

46. W. Froestl *et al.*, SGS742: The first GABAB receptor antagonist in clinical trials. *Biochem. Pharmacol.* **68**, 1479–1487 (2004).

47. K. A. Helm *et al.*, GABAB receptor antagonist SGS742 improves spatial memory and reduces protein binding to the cAMP response element (CRE) in the hippocampus. *Neuropharmacology*.

48, 956–964 (2005).

48. H. A. Born *et al.*, Genetic Suppression of Transgenic APP Rescues Hypersynchronous Network Activity in a Mouse Model of Alzeimer's Disease. *J. Neurosci.* **34**, 3826–3840 (2014).

49. B. Bettler, K. Kaupmann, J. Mosbacher, M. Gassmann, M. Structure, Molecular Structure and Physiological Functions of GABA B Receptors. *Fisiol Rev*. **84**, 835–867 (2004).

50. J. D. Foster, I. Kitchen, B. Bettler, Y. Chen, GABAB receptor subtypes differentially modulate synaptic inhibition in the dentate gyrus to enhance granule cell output. *Br. J. Pharmacol.* **168**, 1808–1819 (2013).

51. G. R. Phillips *et al.*, The presynaptic particle web: Ultrastructure, composition, dissolution, and reconstitution. *Neuron*. **32**, 63–77 (2001).

52. B. De Strooper, L. Umans, F. Van Leuven, H. Van Den Berghe, Study of the synthesis and secretion of normal and artificial mutants of murine amyloid precursor protein (APP): Cleavage of APP occurs in a late compartment of the default secretion pathway. *J. Cell Biol.* **121**, 295–304 (1993).

53. C. Sala Frigerio *et al.*, ??-Secretase cleavage is not required for generation of the intracellular C-terminal domain of the amyloid precursor family of proteins. *FEBS J.* **277**, 1503–1518 (2010).

54. J. de Wit *et al.*, LRRTM2 Interacts with Neurexin1 and Regulates Excitatory Synapse Formation. *Neuron*. **64**, 799–806 (2009).

55. J. N. Savas *et al.*, The Sorting Receptor SorCS1 Regulates Trafficking of Neurexin and AMPA Receptors. *Neuron*. **87**, 764–780 (2015).

56. a J. Link *et al.*, Direct analysis of protein complexes using mass spectrometry. *Nat. Biotechnol.* **17**, 676–682 (1999).

57. M. P. Washburn, D. Wolters, J. R. Yates, Large-scale analysis of the yeast proteome by multidimensional protein identification technology. *Nat. Biotechnol.* **19**, 242–7 (2001).

58. J. N. Savas, B. H. Toyama, T. Xu, J. R. Yates, M. W. Hetzer, Extremely Long-Lived Nuclear Pore Proteins in the Rat Brain. *Science (80-.).* **335**, 942–942 (2012).

59. J. Peng, J. E. Elias, C. C. Thoreen, L. J. Licklider, S. P. Gygi, Evaluation of Multidimensional Chromatography Coupled with Tandem Mass Spectrometry (LC / LC - MS / MS) for Large-Scale Protein Analysis : The Yeast Proteome. *J. Proteome Res.* **2**, 43–50 (2003).

60. D. Cociorva, D. L. Tabb, J. R. Yates, in *Current Protocols in Bioinformatics*, Andreas, D, Baxevanis, Eds. (2007).

61. D. L. Tabb, W. H. McDonald, J. R. Yates, DTASelect and Contrast: Tools for Assembling and Comparing Protein Identifications from Shotgun Proteomics. *J. Proteome Res.* **1**, 21–26 (2002).

62. E. JK, M. AL, Y. JR., An approach to correlate tandem mass spectral data of peptides with amino acid sequences in a protein database. *J Am Soc Mass Spectrom.* **5**, 976–89 (1994).

63. S. Heber *et al.*, Mice with Combined Gene Knock-outs Reveal Essential and Partially Redundant Functions of Amyloid Precursor Protein Family Members. *J. Neurosci.* **20**, 7951–7963 (2000).

64. E. Abramov *et al.*, Amyloid-beta as a positive endogenous regulator of release probability at

hippocampal synapses. *Nat. Neurosci.* **12**, 1567–1576 (2009).

65. A. Delaglio, F.; Grzesiek, S.; Vuister, G. W.; Zhu, G.; Pfeifer, J.; Bax, NMRPipe: a multidimensional spectral processing system based on UNIX pipes. *J. Biomol. NMR*. **6**, 277–293 (1995).

66. E. D. Vranken, W. F.; Boucher, W.; Stevens, T. J.; Fogh, R. H.; Pajon, A.; Llinas, M.; Ulrich, E. L.; Markley, J. L.; Ionides, J.; Laue, The CCPN data model for NMR spectroscopy: development of a software pipeline. *Proteins*. **59**, 687–696 (2005).

67. R. W. Cheung, M. S.; Maguire, M. L.; Stevens, T. J.; Broadhurst, DANGLE: a Bayesian inferential method for predicting protein backbone dihedral angles and secondary structure. *J. Magn. Reson.* **202**, 223–233 (2010).

68. L. Güntert, P.; Buchner, Combined automated NOE assignment and structure calculation with CYANA. *J. Biomol. NMR*. **62**, 453–471 (2015).

69. G. L. Brünger, A. T.; Adams, P. D.; Clore, G. M.; DeLano, W. L.; Gros, P.; Grosse-Kunsteleve, R. W.; Jiang, J.-S.; Kuszewski, J.; Nilges, M.; Pannu, N. S.; Read, R. J.; Rice, L. M.; Simonson, T.; Warren, Crystallography and NMR system (CNS): a new software suite for macromolecular structure determination. *Acta Cryst. Ser. D*. **54**, 901–921 (1998).

70. W. M.P., *The Transferred NOE. In: Webb G.A. (eds) Modern Magnetic Resonance. Springer, Dordrecht.* (2008).

71. G. M. Schwieters, C. D.; Kuszewski, J.; Tjandra, N.; Clore, The Xplor-NIH NMR molecular structure determination package. *J. Magn. Reson*. **160**, 66–7r (2003).

72. H. Dana *et al.*, Thy1-GCaMP6 transgenic mice for neuronal population imaging in vivo. *PLoS One*. **9** (2014), doi:10.1371/journal.pone.0108697.

73. T. A. Pologruto, B. L. Sabatini, K. Svoboda, ScanImage: Flexible software for operating laser scanning microscopes. *Biomed. Eng. Online*. **2**, 1–9 (2003).

74. E. Özkan *et al.*, An extracellular interactome of immunoglobulin and LRR proteins reveals receptor-ligand networks. *Cell*. **154** (2013), doi:10.1016/j.cell.2013.06.006.

75. P. Anton van der Merwe, A. Neil Barclay, Transient intercellular adhesion: the importance of weak protein-protein interactions. *Trends Biochem. Sci.* **19**, 354–358 (1994).

76. S. Blein *et al.*, Structural analysis of the complement control protein (CCP) modules of GABAB receptor 1a: Only one of the two CCP modules is compactly folded. *J. Biol. Chem.* **279**, 48292–48306 (2004).

Acknowledgments:

We thank Genevieve Conway, An Snellinx, Katleen Craessaerts, Katrien Horré, Kristel Vennekens, Véronique Hendrickx, and Jonas Verwaeren for technical help. We thank Charlotte Martin, Nuno Apóstolo, Giuseppe Condomitti, Gabriele Marcassa, and Iordana Chrysidou for experimental assistance. We thank Lieven Buts for help with NMR structure calculations; Marc Aurel Busche for advice on *in vivo* calcium imaging experiments; Patrick Vanderheyden, Sven Zels, Isabelle Beets, Liliane Schoofs, Henry Dunn, Kirill Martemyanov for advice on and/or performing GPCR activity experiments; Ulrike Mueller for the APP/APLP1 KO mice. **Funding:** This work was supported by Alzheimer's Association Research Fellowship AARF-16-442885 (H.C.R.); Stichting Voor Alzheimer Onderzoek Pilot Grant 16011 (H.C.R.); Agency for Innovation by Science and Technology in Flanders IWT 141698 (A.S.); National Science Foundation BRAIN EAGER MCB-1450895 and IOS-1755189 (D.C.); Robert Wood Johnson Foundation Grant #74260 to the Child Health Institute of New Jersey (D.C.); RO1AG061787 (J.N.S.); VUB onderzoeksfonds SRP13 (H.R.); European Research Council (ERC) 724866 (I.S.); FWO Project Grant G.0946.16N (K.F.); Vlaams Initiatief voor Netwerken voor Dementie Onderzoek (VIND, Strategic Basic Research Grant 135043) (B.D.S.); FWO Project Grant G.0D98.17N (B.D.S.); KU Leuven Methusalem Grant (B.D.S. and J.d.W.); ERC Starting Grant 311083 (J.d.W.); FWO Odysseus Grant (J.d.W.); FWO Project Grant G.0654.15N (J.d.W.). B.D.S. is supported by the Arthur Bax and Anna Vanluffelen chair for Alzheimer's disease, "Opening the Future" of the Leuven Universiteit Fonds (LUF) and by the "Geneeskundige Stichting Koningin Elisabeth". **Author contributions:** H.C.R, B.D.S, and J.d.W. conceived the study. All authors planned experiments. H.C.R, D.D.M, A.S., S.F. I.V.M., A.V, E.C., I.V., J.N., F.M.R, and K.D.W.

performed the experiments. All authors interpreted data. H.C.R., B.D.S., and J.d.W. wrote the first version of the manuscript. All authors contributed to and approved the final version. **Competing interests:** H.C.R., B.D.S., and J.d.W. are inventors on a patent on the APP-GABAB receptor interaction that is owned by VIB and the KU Leuven. EP 16180433.1 "Therapeutic agents for neurological and psychiatric disorders." **Data and materials availability:** Resonance assignments were deposited in the BMRB data bank (accession number 27581) and the 20 lowest-energy structures were deposited in the PDB bank (accession code 6HKC).

Supplementary Materials:

Materials and Methods

Figures S1-S10

Tables S1-S4

Movies S1-S2

References (*51-76*)

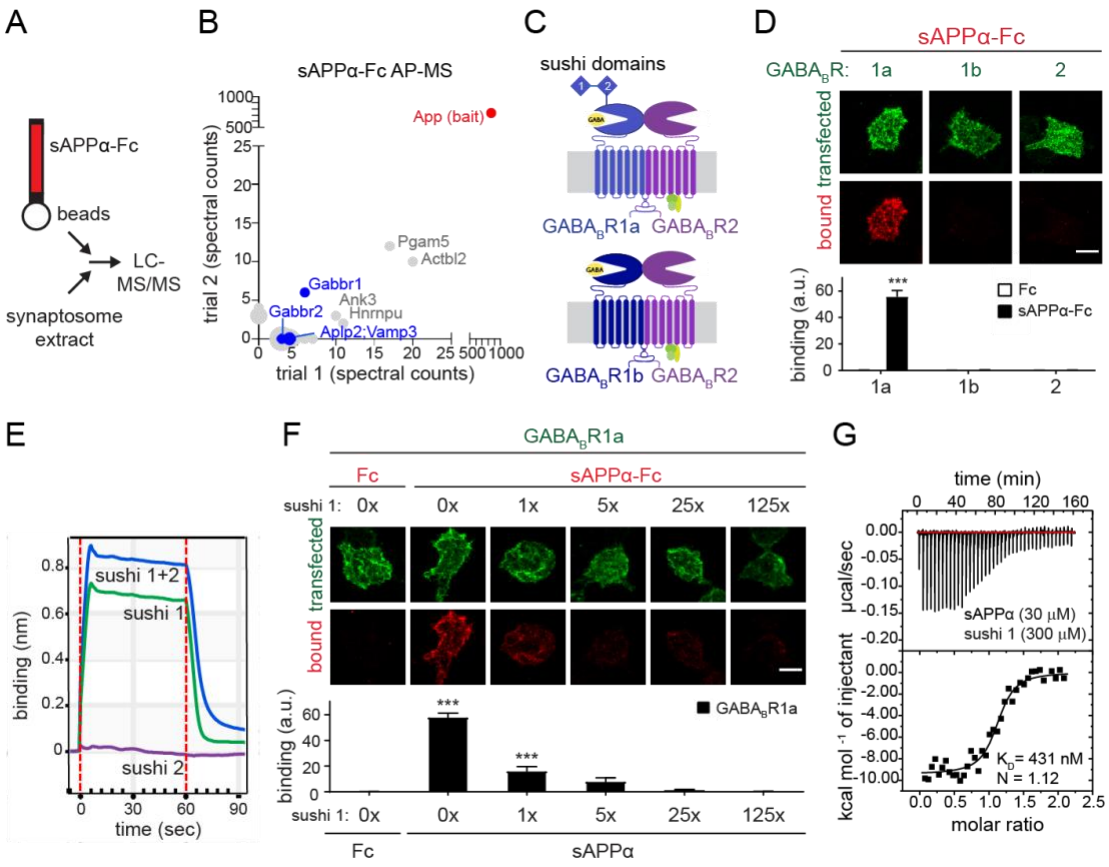

Fig. 1. sAPP selectively binds the sushi 1 domain of GABABR1a

(A) Cartoon illustrating AP-MS workflow. **(B)** Spectral counts of proteins identified by mass spectrometry from 2 independent sAPPα-Fc pull-downs on rat synaptosome extracts. Only proteins which were absent in the Fc controls and present with > 2 spectral counts in a single trial are included. Cell-surface proteins are highlighted in blue. **(C)** Cartoon of GABABR subunits and isoforms. **(D)** Confocal images (upper) and quantifications (lower) of immunostaining for sAPPα-Fc or Fc binding to GABABR1a- , 1b- , or 2-expressing HEK293T cells (n=24). **(E)** Binding of sAPPα purified protein to immobilized Fc-tagged sushi 1, sushi 2, or sushi 1+2 peptides by biolayer interferometry. **(F)** Confocal images (upper) and quantifications (lower) of

immunostaining for Fc control or sAPPα-Fc binding to GABA$_B$R1a-expressing HEK293T cells in the presence of increasing concentrations of untagged sushi 1 peptide (n=24-31). **(G)** Binding of purified sAPPα and sushi 1 proteins (Fc-tag enzymatically removed from both constructs) by isothermal titration calorimetry (ITC). The number of total cells from 3-4 independent experiments is defined by n. Graphs show means ± SEM. Two-way (D) or one-way (F) ANOVA with Bonferroni's post hoc analysis. ***P < 0.001. Scale bar 10 µm.

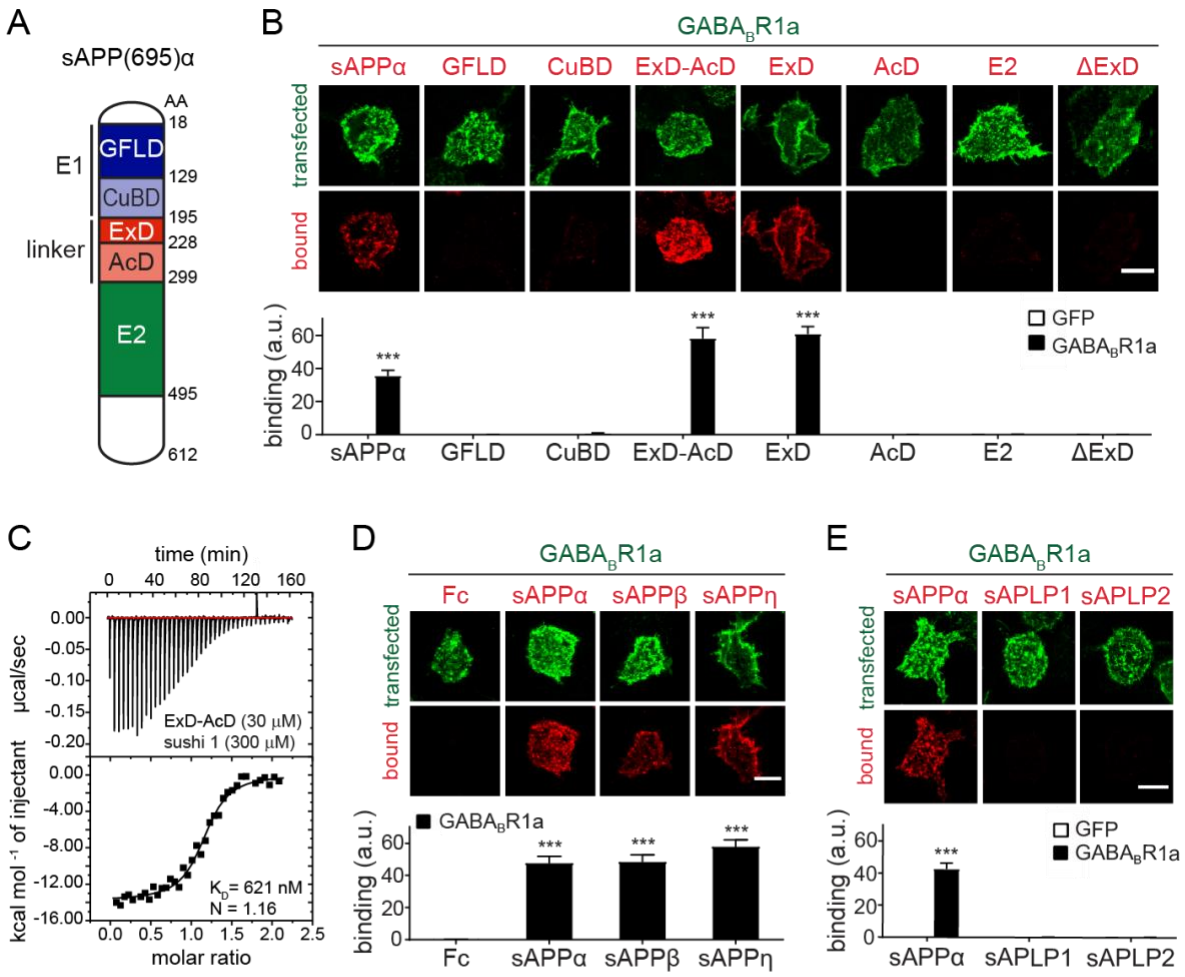

Fig. 2. The extension domain of sAPP binds GABABR1a

(A) Cartoon of sAPPα domains. **(B)** Confocal images (upper) and quantifications (lower) of immunostaining for sAPPα-Fc, GFLD-Fc, CuBD-Fc, ExD-AcD-Fc, ExD-Fc, AcD-Fc, E2-Fc or sAPPαΔExD-Fc binding to GFP- or GABABR1a-expressing HEK293T cells (n=24-32). **(C)** Binding of purified ExD-AcD-Fc and sushi 1 proteins by ITC. **(D)** Confocal images (upper) and quantifications (lower) of immunostaining for Fc control, sAPPα-Fc, sAPPβ-Fc binding to GABABR1a-expressing HEK293T cells (n=24-30). **(E)** Confocal images (upper) and

quantifications (lower) of immunostaining for sAPPα-Fc, sAPLP1-Fc, of sAPLP2-Fc (red) binding to GFP or GABA$_B$R1a-expressing HEK293T cells (green) (n=24). The number of total cells from 3-5 independent experiments is defined by n. Graphs show means ± SEM. Two-way (B,E) or one-way (D) ANOVA with Bonferroni's post hoc analysis. ***P < 0.001. Scale bar 10 µm.

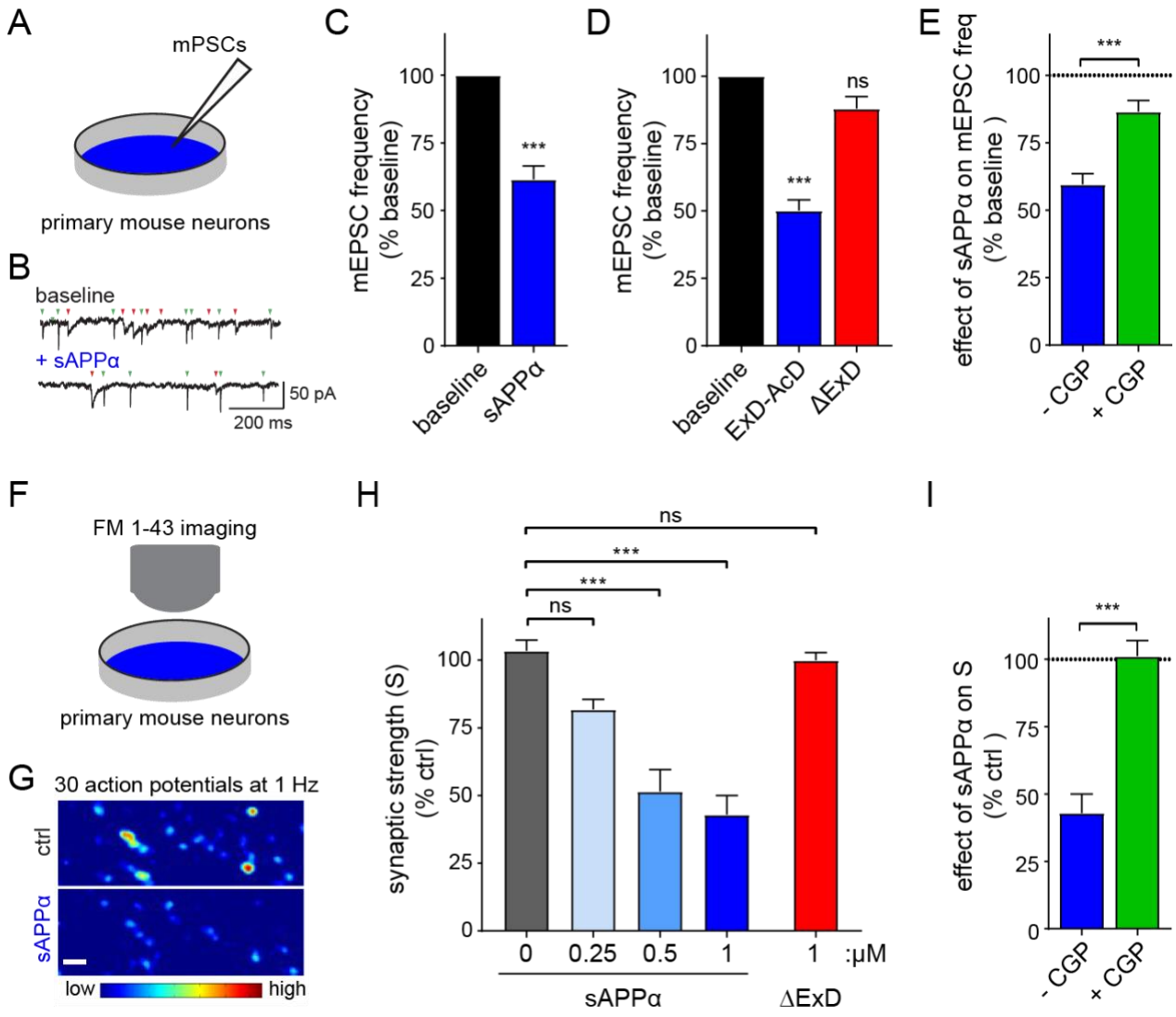

Fig. 3. sAPPα reduces the release probability of synaptic vesicles via presynaptic GABA$_B$R1a

(A) Cartoon of mPSC measurements in cultured hippocampal mouse neurons reported in B-E. **(B,C)** Example traces of mEPSCs (green arrowheads) and mIPSCs (red arrowheads) (B) and average mEPSC frequency (C) normalized to baseline recorded from primary neurons before (baseline) and after treatment with sAPPα (250 nM, Fc-tag enzymatically removed, n=13, N = 3, paired t-test). **(D)** Same as C but with either ExD-AcD, or sAPPαΔExD (Fc-tag enzymatically removed, n=17-20, N=3, one way ANOVA with Dunnett's *post hoc* analysis). **(E)** Same as C but

with sAPP and either without (blue) or with (green) preincubation with CGP55845 (CGP, 5 µM), a $GABA_BR$ antagonist. Dotted line denotes baseline (n=14-17, N=3 unpaired t-test). **(F)** Cartoon of FM1-43 measurements in cultured hippocampal mouse neurons reported in G-I. **(G)** High-magnification ΔF images before and after application of sAPPα (Fc-tag enzymatically removed, 1 µM) to primary neurons. **(H)** Summary of the dose-dependent inhibitory effect of sAPPα on presynaptic strength (S) (N= 5-8, one way ANOVA analysis with *post hoc* Tukey's analysis). **(I)** Summary of sAPPα effect on presynaptic vesicle recycling in hippocampal neurons with or without CGP (normalized to control (ctrl)) (N =8). The number of neurons is defined as n, and the number of independent experiments or mice is defined as N. Graphs show means ± SEM. * $P < 0.05$, ** $P < 0.1$ *** $P < 0.001$.

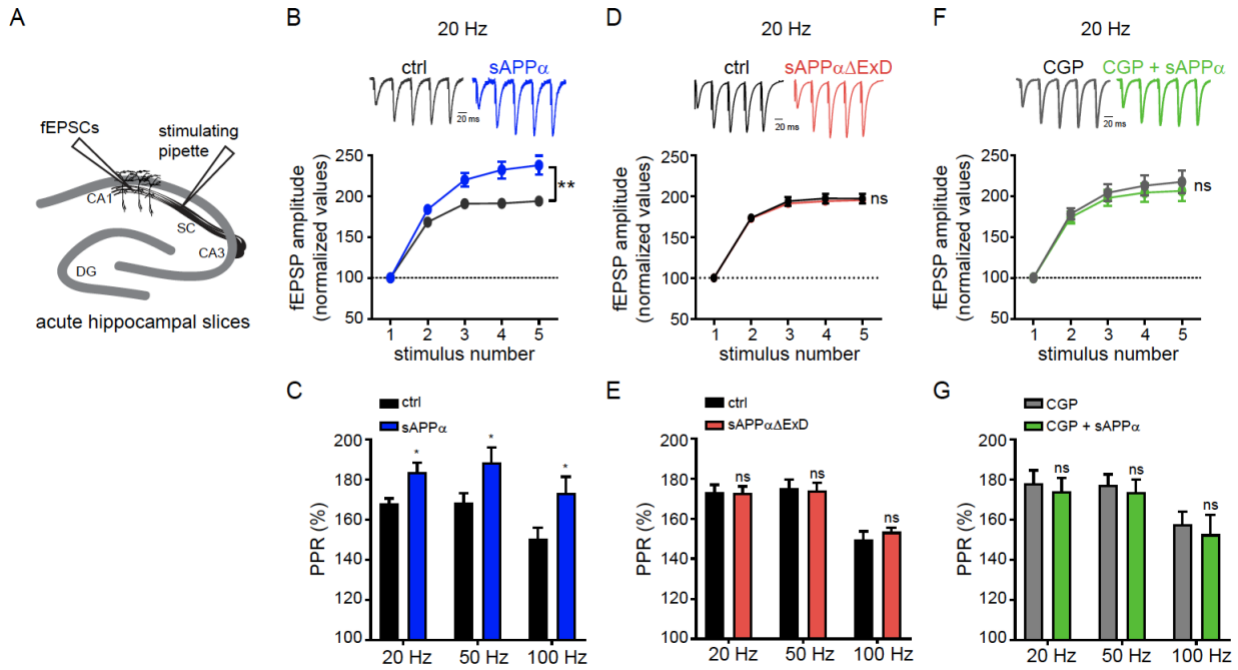

Fig. 4. sAPP enhances short-term plasticity at Schaffer collateral synapses in a GABAʙR1a-dependent manner

(A) Cartoon of fEPSC measurements in acute mouse hippocampal slices reported in B-G. **(B)** Representative traces (upper) and average fEPSP amplitude (lower) recorded at Schaffer collaterals (SC) in response to high-frequency burst stimulation at 20 Hz in mouse hippocampal slices incubated without (n = 12, N = 7) or with sAPPα (1 µM, Fc-tag enzymatically removed) (n = 10, N = 7). fEPSPs were normalized to the peak amplitude of the first response. **(C)** Paired-pulse ratios (PPR) for the first two pulses at each frequency (20 Hz, 50 Hz, and 100 Hz). **(D)** Same as B but in slices incubated without (n = 10, N = 4) or with sAPPαΔExD (1 µM, Fc-tag enzymatically removed, n = 9, N = 4). **(E)** Same as C. **(F)** Same as B but in slices incubated with CGP 54626 (CGP, 10µM) alone (n = 9, N =4) and slices incubated with CGP + sAPPα (n = 8, N = 4). **(G)** Same as C. The number of slices is defined as n, and the number of independent experiments or

mice is defined as N. Graphs show means ± SEM. * P < 0.05, ** P < 0.1 *** P < 0.001. Two-way ANOVA analysis.

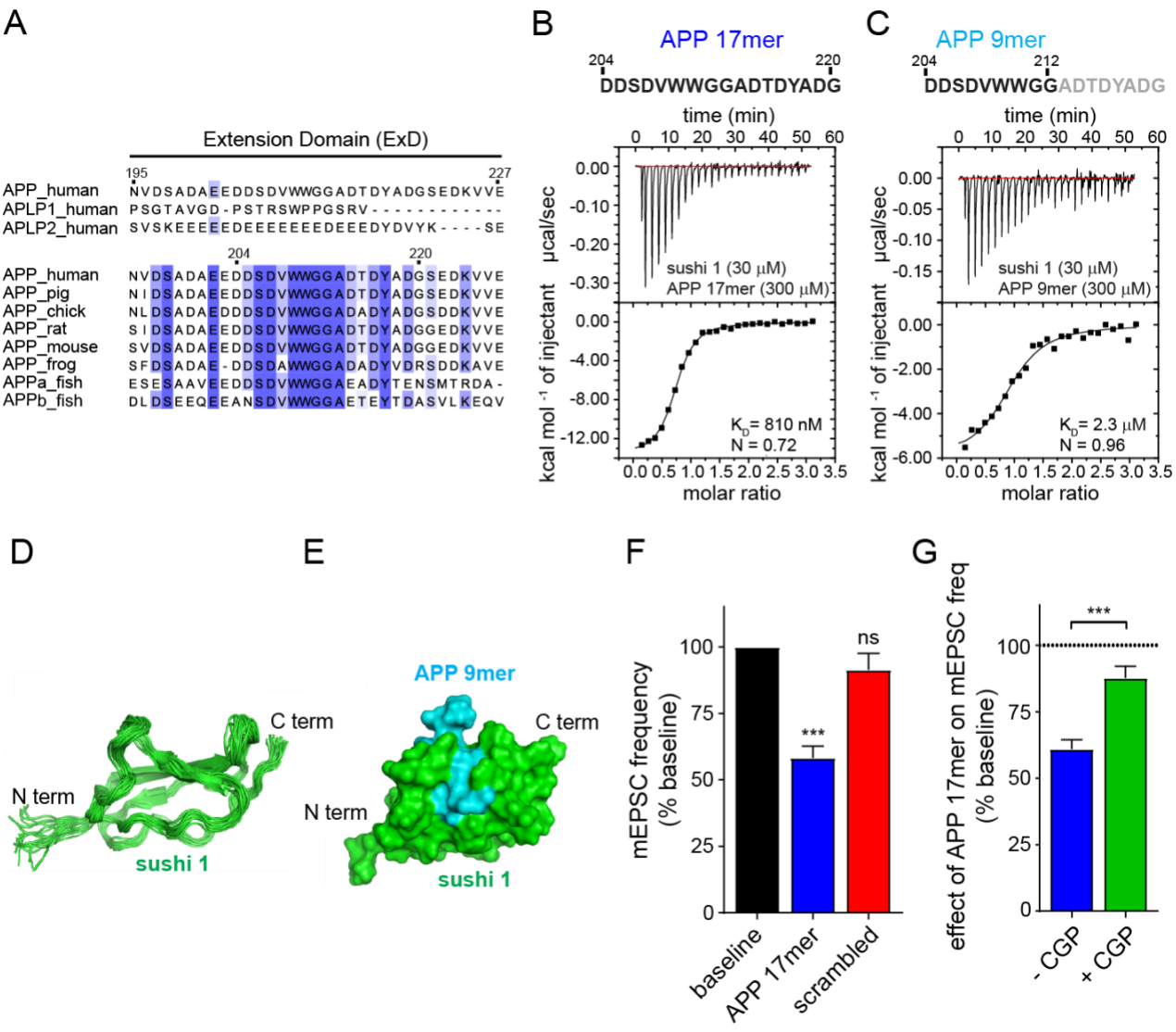

Fig. 5. A short peptide within the APP ExD suppresses synaptic vesicle release via GABABR1a

(A) Sequence alignment for the extension domain (ExD) of human APP with APLPs and with 7 vertebrate APP sequences. **(B,C)** ITC binding experiments of purified sushi 1 and synthetic peptides within the ExD corresponding to (B) 204-220AA or (C) 204-212AA of APP695. **(D)** An ensemble of 20 lowest-energy NMR structures of the sushi 1 domain of GABABR1a when bound to the APP 9mer peptide. **(E)** A structural model of the complex between the sushi 1 domain of

GABA$_B$R1a (green) and the APP 9mer peptide (cyan) shown as the molecular surface. Protein termini are indicated by the labels. **(F)** Average mEPSC frequency normalized to baseline recorded from mouse primary neurons before (baseline) and after treatment with 17mer APP peptide (250 nM, APP695 204-220AA) (n= 20, N=3) or scrambled 17mer control peptide (250 nM, n= 18, N= 4) (one way ANOVA with Dunnett's *post hoc* analysis). **(G)** Quantification of the effect of 250 nM 17mer APP peptide (APP695 204-220AA) on mEPSC frequency normalized to baseline (K) either without (n=14; N=3) or with preincubation with CGP55845 (CGP, 5 µM; n=16, N=3) (unpaired t-test). Dotted line denotes baseline. The number of neurons is defined by n. The number of independent experiments is defined by N. Graphs show means ± SEM. * $P < 0.05$, ** $P < 0.1$ *** $P < 0.001$.

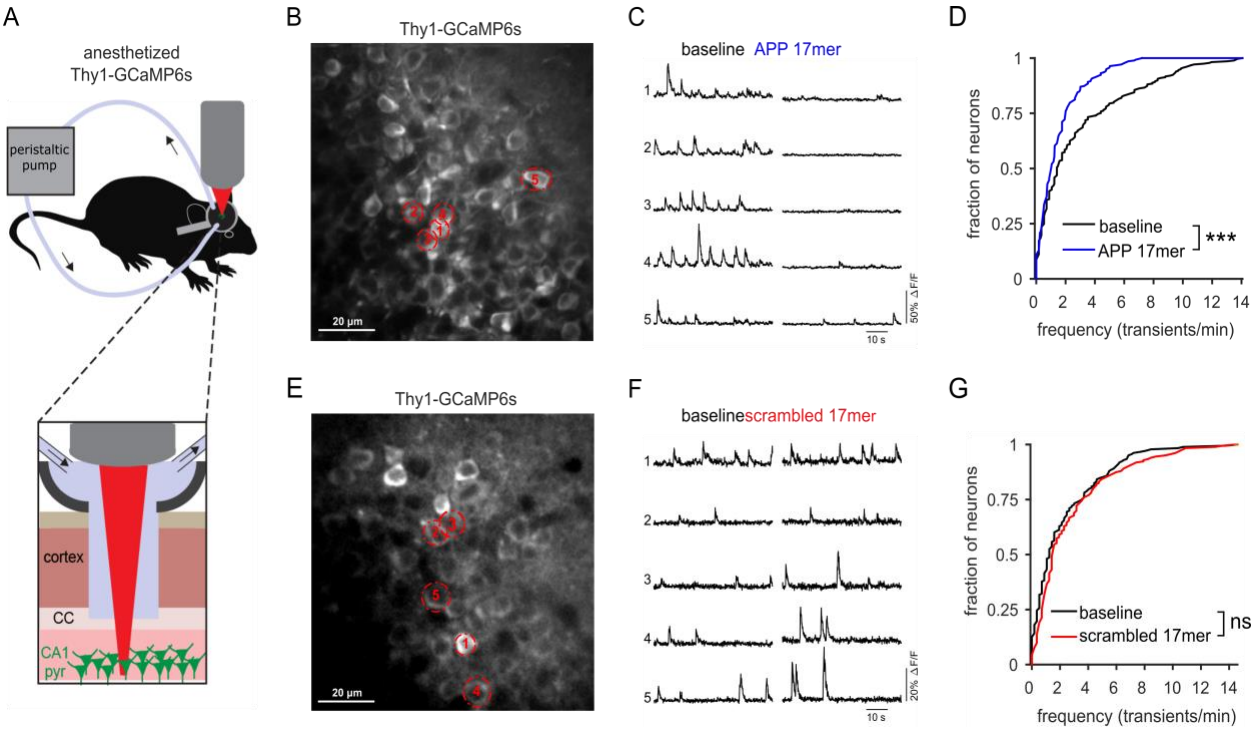

Fig. 6. A 17AA peptide corresponding to the GABABR1a binding region within APP suppresses neuronal activity *in vivo*

(A) Cartoon of *in vivo* 2-photon calcium imaging of CA1 hippocampus of anesthetized Thy1-GCaMP6s mice with superfusion of APP 17mer, or scrambled control 17mer. **(B)** *in vivo* image of CA1 hippocampal neurons of Thy1-GCaMP6s mice. Representative neurons indicated with dotted outline. **(C)** Calcium traces of five representative neurons, labeled in panel A, before (baseline) and during bath application of 5 µM APP 17mer peptide corresponding to the GABABR1a binding region within APP (APP 17mer). **(D)** Cumulative distribution of the frequency of calcium transients at baseline (black line) and during APP 17mer bath application (blue line) (n=277; N=3). **(E)** *in vivo* image of CA1 hippocampal neurons of Thy1-GCaMP6s mice. **(F)** Calcium traces of five representative neurons, labeled in panel D, before (baseline) and during bath application of 5µM scrambled 17mer control peptide (scrambled 17mer). **(G)** Cumulative

distribution of the frequency of calcium transients at baseline (black line) and during scrambled 17mer bath application (red line) (n=183; N=3). Wilcoxon rank sum test. The number of neurons is defined by n. The number of mice is defined by N. *** $P < 0.001$; NS $P>0.05$

5

Supplementary Materials for

Secreted Amyloid-β Precursor Protein Functions as a GABABR1a Ligand to Modulate Synaptic Transmission

Heather C. Rice[1,2], Daniel de Malmazet[3,4], An Schreurs[5], Samuel Frere[6], Inge Van Molle[7], Alexander N. Volkov[7,8], Eline Creemers[1,2], Irena Vertkin[6], Julie Nys[1,2], Fanomezana M. Ranaivoson[9], Davide Comoletti[9], Jeffrey N. Savas[10], Han Remaut[7], Detlef Balschun[5], Keimpe D. Wierda[1,2], Inna Slutsky[6], Karl Farrow[3,4,11,12], Bart De Strooper[1,2,13,]*, and Joris de Wit[1,2,]*

*Correspondence to: bart.destrooper@kuleuven.vib.be; joris.dewit@kuleuven.vib.be

This PDF file includes:

Other Supplementary Materials for this manuscript include the following:

Movies S1 to S2

5

Materials and Methods

Animals

All animal experiments were conducted according to the KU Leuven and Tel Aviv University ethical guidelines and approved by the KU Leuven or the Tel Aviv University Committee on Animal Care.

Plasmids

APP-Fc constructs were generated by PCR-amplifying the following regions of mouse APP695: sAPPα= 18-612aa; sAPPβ= 18-596aa; GFLD= 18-128aa; CuBD= 129-194aa; AcD-Exd=195-298aa; ExD= 195-227aa; AcD= 228-298aa; E2= 299 – 494aa; sAPPαΔExD= 19-194aa & 228-596aa. APLP-Fc constructs were generated by PCR-amplifying the ectodomain without the signal sequence of mouse APLP1 (38-583aa) and mouse APLP2 (32-636aa). Each of the PCR fragments were subcloned between and in frame with the prolactin signal peptide and human Fc in the pCMV6-XL4 vector using Gibson Assembly (NEB).

The cDNA clone for human GABAʙR2 was obtained from the cDNA Resource Center and the cDNA clone for human GABAʙR1b was obtained from Origene. The N-terminal domain lacking the signal sequence was synthesized for GABAʙR1a or generated by PCR-amplification for GABAʙR1b and GABAʙR2. The fragments were subcloned into pDisplay (Invitrogen), making a fusion protein with the transmembrane domain of the platelet derived growth factor receptor and an N-terminal HA epitope tag.

Biochemical fractionation

Seven P21 rat brains were homogenized in homogenization buffer (0.32 M Sucrose, 1 mM $NaHC0_3$, 1mM $MgCl_2$, 0.5 mM $CaCl_2$) with protease inhibitor using a glass Dounce homogenizer. "Homogenates" were centrifuged at 1000 x g for 15 minutes at 4°C. Postnuclear supernatants were centrifuged at 10,000 x g for 20 minutes. The pellet P2 containing "crude membranes" was resuspended in Solution B (0.32 M sucrose, 1mM NaHC03, with protease inhibitors) and loaded onto sucrose gradient (1.2M, 1M, .5M sucrose) and centrifuged at 32,500 x g for 2 hrs. Pure

"synaptosome" was collected from between the 1.2M and 1M sucrose interphase. Synaptosomes were diluted in Buffer B and 0.5% Triton X-100, incubated for 30 minutes at 4°C to enrich for presynaptic proteins (*51*), and centrifuged at 32,500 x g for 25 mins to yield a supernatant with "triton soluble" synaptosomes. Pellet was resuspended in Buffer B and loaded on a second sucrose gradient (2M, 1.5M, 1M sucrose) and centrifuged at 200,000g for 2 hrs. Triton insoluble fraction was collected from between the 1.5M and 2M sucrose interface and centrifuged at 200,000g for 20 mins. The pellet was then resuspended as the final "triton insoluble" fraction. Protein content was quantified in each fraction by Pierce BCA protein assay (Thermo Fisher) and equal protein amounts were loaded onto SDS-PAGE and immunoblotted using the following primary antibodies: rabbit anti-APP (c-terminal, B63, (*52*)), rabbit anti-APLP1 (W1CT, gift of Dominic Walsh (*53*)); rabbit anti-APLP2 (W2CT, gift of Dominic Walsh (*53*)), mouse anti-synaptophysin (Sigma), mouse anti-PSD-95 (Thermo Scientific), and mouse anti-NR2A (BD Biosciences).

Immunohistochemistry

P35 C57/Bl6 wild type mice were transcardially perfused with 4% paraformaldehyde. Brains were dissected, post fixed with 4% paraformaldehyde for 1 hour, cryopreserved in 30% sucrose solution, and embedded in Tissue-Tek® OCT for freezing. Coronal cryosections were prepared with 16 μm thickness. Sections were permeabilized and blocked at RT for 2 hours in PBS, 0.5% Triton X-100, 10% normal horse serum, and incubated with the primary antibody at 4˚C O/N followed by 2 hr incubation with Fluorophore-conjugated secondary antibodies (Jackson ImmunoResearch or Invitrogen). The following primary antibodies were used: rabbit anti-APP (c-terminal, B63, (*52*)), guinea pig anti-VGLUT1 (Millipore), mouse anti-PSD-95 (Thermo Scientific), guinea pig anti-VGAT (Synaptic Systems), mouse anti-Gephyrin (Synaptic Systems). Fluorophore-conjugated secondary antibodies were from Jackson ImmunoResearch or Invitrogen. Images were acquired by super-resolution structured illumination microscopy on a Zeiss Elyra S.1.

Protein expression and purifications from HEK293T cells

Secreted C-terminally Fc-tagged proteins were expressed by stable or transient transfection (using PEI transfection reagent) in HEK293T cells and collected in serum-free Opti-MEM (Thermo Fisher Scientific, Inc.). For Fc-tagged proteins used in the proteomics screen and cell-surface binding assays, conditioned medium was run on an affinity column packed with Protein-G Plus Agarose fast flow resin (Pierce) using a gravity-flow system. Affinity column was washed with 250 ml wash buffer (50 mM HEPES pH 7.4, 300 mM NaCl) and eluted with 10 ml IgG elution buffer (Pierce). For non-Fc proteins used in functional and in vitro binding assays, following passage of conditioned medium through the column packed with Protein-G Agarose, the column was washed with 250 mL wash buffer (50mM Tris pH 8.0, 450 mM NaCl, 1 mM EDTA), the Fc tag was cleaved by O/N incubation with GST-tagged 3C PreScission Protease (GE Healthcare) in cleavage buffer (50mM Tris pH 8.0, 150 mM NaCl, 1 mM EDTA, 1 mM DTT) , and the cleaved protein was collected in the eluate. The protease was subsequently separated from the eluted proteins using a Glutathione Sepharose (GE Healthcare) packed column. Proteins were concentrated using Amicon Ultra 10 kDa MWCO centrifugal filter units (Millipore) (or other appropriate MW cut off), dialyzed against PBS, and protein concentration determined by Bradford assay (Bio-Rad).

Sushi 1 expression and purification from bacteria

For biophysical and structural biology purposes the Sushi1 protein was expressed in a bacterial expression system. The synthetic gene encoding for residues 26-96 of the Sushi1 protein was cloned into a pFloat-SUMO vector, generating a His-tagged SUMO-Sushi1 fusion protein. The construct also contained a 3C protease cleavage site to remove the His-SUMO-tag. The pFloat-SUMO-Sushi1 plasmid was transformed in BL21(DE3) cells and plated on kanamycin (100 µg/ml) containing LB agar plates. A small LB culture, supplemented with 100 µg/ml kanamycin, was inoculated with a single colony of BL21(DE3)(pFloat-SUMO-Sushi1) and grown overnight at 37°C. 1L LB cultures were subsequently inoculated with 20 ml of this preculture and grown at 37°C until OD600 reached 0.8. At this point, protein expression was induced using 0.5 mM isopropyl β-D-1-thiogalactopyranoside (IPTG). Cells were incubated further overnight at 20°C and subsequently harvested by centrifugation (Beckman rotor 8.1000, 5000 rpm, 15 min, 4°C). The pellet was resuspended in 20 mM Tris pH 7.5, 500 mM NaCl, 10 mM imidazole, 5 mM ß-mercaptoethanol, 0.1 mg/mL 4-(2-aminoethyl) benzenesulfonyl fluoride hydrochloride (AEBSF), 1 µg/mL leupeptin, 50 µg/mL DNaseI

and 20 mM $MgCl_2$. The cells were lysed using a French press (Constant Systems) at 20 kpsi and the cell debris was removed by centrifugation. The cell lysate was loaded on a Ni-sepharose FF HiLoad column (GE Healthcare), equilibrated in 20 mM Tris pH 7.5, 500 mM NaCl, 10 mM imidazole, 5 mM ß-mercaptoethanol. The bound proteins were eluted using a linear gradient to 500 mM imidazole. Fractions containing the His-SUMO-Sushi1 protein were pooled and dialysed overnight to 20 mM Tris pH 7.5, 150 mM NaCl, while cleaving with 3C protease. The cleaved sample was loaded again on a Ni-sepharose FF HiLoad column, equilibrated in the same buffer. The FT, containing the Sushi1 protein, was concentrated and applied to a BioRad S100 16/60 size exclusion column, equilibrated in 50 mM KPi buffer pH 6.0, 50 mM NaCl.

For expression of $^{13}C/^{15}N$ labelled Sushi1, cultures were grown in 500 mL Min9 medium (6.8 g/L Na_2HPO4, 3 g/L KH_2PO4, 1 g/l NaCl) supplemented with 50 mg/L EDTA, 0.2 mg/L H_3BO_3, 3 mg/L $CuCl_2 \cdot 2H_2O$, 7 mg/L $ZnSO_4 \cdot 7H_2O$, 8 mg/L $CoCl_2 \cdot 6H_2O$, 12 mg/mL $MnCl_2 \cdot 4H_2O$, 60 mg/L $FeSO4 \cdot 7H_2O$, 2 mM MgSO4, 0.2 mM $CaCl_2$, 2.5 g/L ^{13}C glucose, 1 g/L $^{15}NH_4Cl$ and 50 µg/ml kanamycin (inoculated with 1 ml of LB preculture) instead of LB. All other steps of the expression and purification protocol were unchanged.

$^{13}C/^{15}N$ labelled APP 9mer peptide expression and purification

In order to be able to express $^{13}C/^{15}N$ labelled APP 9mer peptide, the peptide was cloned in a pFloat-SUMO vector to obtain the 3C protease cleavable His-SUMO-APP9 construct. The pFloat-SUMO-APP9 plasmid was transformed in C43(DE3) competent cells and plated on kanamycin (100 µg/ml) containing LB agar plates. A small LB culture, supplemented with 100 µg/ml kanamycin, was inoculated with a single colony of C43(DE3)(pFloat-SUMO-APP9) and grown overnight at 37°C. 500 mL cultures in Min9 supplemented with EDTA, H_3BO_3, $CuCl_2 \cdot 2H_2O$, $ZnSO_4 \cdot 7H_2O$, $CoCl_2 \cdot 6H_2O$, $MnCl_2 \cdot 4H_2O$, $FeSO_4 \cdot 7H_2O$, $MgSO_4$, $CaCl_2$, ^{13}C glucose, $^{15}NH_4Cl$ and kanamycin (concentrations as indicated above) were subsequently inoculated with 1 ml of this preculture and grown at 37°C until OD600 reached 0.8. At this point protein expression was induced using 0.5 mM isopropyl β-D-1-thiogalactopyranoside (IPTG). Cells were incubated further overnight at 20°C and subsequently harvested by centrifugation (Beckman rotor 8.1000, 5000 rpm, 15 min, 4°C).

The pellet was resuspended in PBS, 10 mM imidazole, 5 mM ß-mercaptoethanol, 0.1 mg/mL 4-(2-aminoethyl) benzenesulfonyl fluoride hydrochloride (AEBSF), 1 µg/mL leupeptin, 50 µg/mL DNaseI and 20 mM $MgCl_2$. The cells were lysed using a French press (Constant Systems) at 20 kpsi and the cell debris was removed by centrifugation. The cell lysate was loaded on a Ni-sepharose FF HiLoad column (GE Healthcare), equilibrated in PBS, 10 mM imidazole, 5 mM ß-mercaptoethanol. The bound proteins were eluted using a linear gradient to 500 mM imidazole. Fractions containing the His-SUMO-APP9 protein were pooled, concentrated, and buffer exchanged to PBS buffer. Following 2 hr 3C protease digestion, the protein was again loaded on a Ni-sepharose FF HiLoad column, equilibrated in the same buffer. The flow-through (FT), containing the APP 9 peptide, was lyophilized. The crude residue was dissolved in a mixture of water and acetonitrile (1:1). The resulting solution was purified using a semi-preparative HPLC system (KNAUER system) accommodated with a ReproSil-Pur 120 ODS-3 5µm phase C18 column. The flow rate was 10 mL/min using milliQ-water and acetonitrile (both containing 0.1% of trifluoroacetic acid) as solvent system. The gradient used started with 10% of acetonitrile up to 70% over a time span of 10 minutes. Fractions containing the pure product were combined and lyophilized. The final peptide was obtained as a TFA salt with a purity > 95%.

The pure peptide was analyzed by electrospray ionization mass spectroscopy on a Micromass Q-Tof micro system coupled to a Waters Breeze analytical HPLC system equipped with Waters 2489 UV/visible detector (at a wavelength of 215 nm). Electrospray data were acquired on Electrospray positive ionization mode scanning over the mass-to-charge ratio (m/z) scale from 100 to 2000 at a scan time of 1 s, and a cone voltage of 38 V. Data collection was done with Masslynx software.

Formula: $C_{53}H_{67}N_{13}O_{19}$; MW: 1256.24 g/mol; LC-MS (ESI+): 1256.74.

Affinity Chromatography for Mass Spectrometric Identification of sAPP-binding proteins

Affinity chromatography for mass spectrometric identification of binding partners was performed as described previously (*54*, *55*). For each Fc bait, three rat brains were homogenized in homogenization buffer (4 mM HEPES, 0.32 M sucrose) with protease inhibitors using a glass Dounce homogenizer. Homogenates were centrifuged at 1000 x g for 25 mins at 4°C. Supernatants were centrifuged at 14,000 x g for 25 mins at 4°C. The pellet P2 containing crude

synaptosomes was resuspended in homogenization buffer and centrifuged at 10,000 g for 20 mins, yielding pellet P2' containing washed crude synaptosomes. Pellet P2' was extracted in 20 mM Tris pH 8.0, 0.1 mM $CaCl_2$ and 1% Triton X-100 for 2.5 hours at 4°C.The extracts were centrifuged at 100,000 x g for 1 hour, and the final supernatants were collected for affinity chromatography. Protein-G Plus Agarose fast flow resin (Pierce) (Pierce, 500 µl slurry) pre-coupled to 100 µg human Fc control protein, sAPPα-Fc or sAPPβ-Fc, was added to synaptosome extracts and rotated O/N at 4°C. The agarose resin with bound proteins was then packed into Poly-Prep chromatography columns (BioRad) and washed with 50 ml of high-salt wash buffer (50 mM Hepes pH 7.4, 300 mM NaCl, 1 mM EDTA) with protease inhibitors, followed by a wash with 10 ml low-salt wash buffer (50 mM Hepes pH 7.4, 150 mM NaCl, 1 mM EDTA) with protease inhibitors). Bound proteins were eluted from the beads by incubation with Pierce elution buffer and TCA precipitated O/N. For the MS analysis, only proteins with more than two spectra counts from a single pull-down were included, and any proteins that had one or more spectra counts in the Fc controls were excluded. Finally, the dataset was filtered to only include transmembrane, cell-surface proteins using Panther and Uniprot databases.

MudPIT (LCLC-MS/MS) LTQ XL Mass Spectrometry analysis

Protein precipitates were solubilized in 8 M urea and processed with ProteasMAX (Promega) per the manufacturer's instruction. The samples were subsequently reduced by TCEP (tris(2 carboxyethyl)phosphine, 5 mM, room temperature, 20 min), alkylated in the dark by 10 mM iodoacetamide (10 mM, 20 min), digested with Sequencing Grade Modified Trypsin (Promega) overnight at 37 °C, and the reaction was stopped by acidification to 5% final with formic acid.

The entire protein digest was pressure-loaded into a 250-µm i.d capillary packed with 2.5 cm of 10-µm Jupiter C18 resin (Phenomenex) followed by an additional 2.5 cm of 5-µm Partisphere strong cation exchanger (Whatman) (*56*, *57*). The column was washed with buffer containing 95% water, 5% acetonitrile, and 0.1% formic acid. After washing, a 100-µm i.d capillary with a 5-µm pulled tip packed with 15 cm of 4-µm Jupiter C18 resin (Phenomenex) was attached to the filter union and the entire split-column (desalting column–union–analytical column) was placed in line with an Agilent 1200 quaternary HPLC and analyzed using a modified 6-step separation described previously

(*58*). The buffer solutions used were 5% acetonitrile / 0.1% formic acid (buffer A), 80% acetonitrile / 0.1% formic acid (buffer B), and 500 mM ammonium acetate / 5% acetonitrile / 0.1% formic acid (buffer C).

MS analysis was performed on a LTQ XL mass spectrometer using a standard data dependent acquisition strategy with the following settings: MS1 scan range was from 300-2000 M/Z. We used CID fragmentation with a minimal signal required for selection for MS/MS of 1000, an isolation width 2.0, and Normalized collision energy of 35.0. The default charge state setting was set to 2, we rejected charge 1 ions and activation (Q) of 0.25 with an activation time of 30.0. Tthe top 5 most intense peaks were considered for MS/MS.

Analysis of Tandem Mass Spectra

Protein identification and quantification and analysis were done with Integrated Proteomics Pipeline - IP2 (Integrated Proteomics Applications, Inc., San Diego, CA. (http://www.integratedproteomics.com/) using ProLuCID, DTASelect2, Census, and QuantCompare. Spectrum raw files were extracted into ms1 and ms2 files using RawExtract 1.9.9, and the tandem mass spectra were searched against Uniprot mouse protein databases (downloaded on April 1, 2013). In order to accurately estimate peptide probabilities and false discovery rates, we used a target / decoy database containing the reversed sequences of all the proteins appended to the target database (*59*). Tandem mass spectra were matched to sequences using the ProLuCID (modified Sequest) algorithm with 3000 ppm peptide mass tolerance for precursor ions and 600 ppm for fragment ions. ProLuCID searches were done on an Intel Xeon cluster running under the Linux operating system. The search space included all fully- and half-tryptic peptide candidates that fell within the mass tolerance window with no miscleavage constraint. Carbamidomethylation (+57.02146 Da) of cysteine was considered as a static modification. The validity of peptide/spectrum matches (PSMs) was assessed in DTASelect (*60*, *61*), using two SEQUEST(*62*) defined parameters, the crosscorrelation score (XCorr), and normalized difference in cross-correlation scores (DeltaCN). The search results were grouped by charge state (+1, +2, +3, and greater than +3) and tryptic status (fully tryptic, half-tryptic, and nontryptic), resulting in 12 distinct sub-groups. In each one of these sub-groups, the distribution of Xcorr, DeltaCN,and DeltaMass values for (a) direct and (b) decoy database PSMs was obtained, then the direct and decoy subsets were separated by discriminant analysis. Full separation of the direct and decoy PSM subsets is not generally possible; therefore, peptide match probabilities were calculated based on a

nonparametric fit of the direct and decoy score distributions. A peptide confidence of 0.95 was set as the minimum threshold. The false discovery rate was calculated as the percentage of reverse decoy PSMs among all the PSMs that passed the confidence threshold. Each protein identified was required to have a minimum of two peptides and have at least one tryptic terminus. After this last filtering step, we estimate that both the protein false discovery rates were below 1% for each sample analysis.

Cell surface binding assay

HEK293T cells were transfected with GFP (as negative control) or pDisplay-GABABR-1a, -1b, or -2 plasmids using Fugene6 (Promega). Twenty-four hours after transfection, the cells were incubated with Fc (as negative control) or the various Fc-tagged APP proteins (500 nM, in Dulbecco's modified Eagle's medium [DMEM] supplemented with 20 mM HEPES [pH 7.4]) for 1 hr at RT. After three brief washes with DMEM/20 mM HEPES (pH 7.4), cells were fixed in 4% paraformaldehyde, 4% sucrose in PBS. Cells were blocked in 3% BSA in PBS, and staining was performed in detergent-free conditions without cell permeabilization. Primary antibody mouse anti-HA (Covance) was used to detect HA-tagged GABABR-transfected cells. Cy3-conjugated donkey anti-human IgG (Jackson ImmunoResearch) was used to detect bound Fc proteins. Fluorophore-conjugated secondary antibodies were from Jackson ImmunoResearch or Invitrogen. Images were captured on a Leica SP5 confocal microscope (Leica Microsystems, Bannockburn, IL). Image thresholding was set with ImageJ software using constant settings per experiment and the area of Fc binding was measured relative to cell area.

Biolayer Interferometry (BLI)

BLI binding experiments were conducted using a BLItz instrument (ForteBio, Menlo Park, CA) at room temperature. Anti-human Fc capture Biosensors were pre-wetted for 10 min in 300 µl of 10 mM Hepes, pH 7.4, 150 mM NaCl, 5 mM $CaCl_2$, 5mM $MgCl_2$, and 1% (w/v) BSA buffer prior to use. Subsequently, the sensor tips were incubated for 10 minutes with conditioned medium of HEK293T cells transiently transfected with Sushi-1, -2, or -

1&2-Fc, to capture the expressed protein. The binding reaction occurred in a 4 µl drop containing purified sAPPa at 93µM, under agitation. Both association and dissociation were allowed to occur for 60 s. Nonspecific binding and instrument noise were subtracted by using a sensor tip saturated with Fc fragment alone.

Isothermal titration calorimetry (ITC)

All ITC experiments were carried out on a MicroCal *iTC200* system. For ITC experiments involving APP constructs expressed in HEK293T cells, the purified GABA$_B$R1a-Sushi1 domain, sAPPα, CuBD-AcD, AcD and CuBD constructs were buffer-exchanged by size exclusion chromatography in 20 mM Na-HEPES pH 7.0, 150 mM NaCl and 5 mM $CaCl_2$. Concentrated samples were diluted and degassed before the experiment at the concentrations reported in the Figure legends. sAPP fragments (all of them at 30 µM) were placed in the MicroCal sample cell and matching buffer was placed in the reference cell. Sushi1 (300 µM) was in the syringe and was injected into the cell in a series of 1 µL injections at 25°C. All the datasets were subtracted with a reference dataset consisting of serial injections of Sushi1 in the cell, containing buffer only, under the same conditions.

For ITC experiments involving synthetic APP peptides, the Sushi1 protein was dialysed overnight to PBS buffer. The 17-mer APP peptide was resuspended in H_2O:acetonitrile (5:1) at a stock concentration of 3 mM, and diluted in PBS to 300 uM. In order to avoid buffer-buffer mismatches, the same amount of H_2O:acetonitrile mixture was also added when diluting the Sushi1 protein to a 30 uM concentration. The 9-mer APP peptide was resuspended in PBS. Titrations comprised 26 × 1.5 µL injections of peptide into the protein, with 90 s intervals. An initial injection of ligand (0.5 µL) was made and discarded during data analysis.

The raw ITC data were fitted to a single binding site model using the Microcal LLC ITC200 Origin software provided by the manufacturer.

Primary Neurons

Hippocampal neurons were cultured from E18 C57/Bl6 wild type mice or APP/APLP1 double knock out (dKO) mice (provided by Ulrike Müller (*63*)) and plated on poly-D-lysine (Millipore), and laminin (Invitrogen) coated coverslips (Nalge Nunc International). Neurons were maintained in Neurobasal medium (Invitrogen) supplemented with B27, glutamax, penicillin/streptomycin (Invitrogen) and β-mercaptoethanol.

Electrophysiological recordings of cultured mouse neurons

Single neurons from wild type or APP/APLP1 null mutant embryos (E18) were recorded at DIV 12-15. The intracellular whole-cell pipette medium contained (in mM): 136 KCl, 18 HEPES, 4 Na-ATP, 4.6 $MgCl_2$, 15 Creatine Phosphate, 1 EGTA and 50 U/ml Phospocreatine Kinase (300 mOsm, pH 7.30). Regular external solution contained 2 mM/ 2 mM Ca^{2+}/ Mg^{2+} (in mM: 140 NaCl, 2.4 KCl, 2 $CaCl_2$, 2 $MgCl_2$, 10 HEPES, 14 Glucose (300 mOsm, pH 7.30)) and TTX (1 µM). Pharmacological reagents (30 µM baclofen, 5 µM CGP), sAPLP1, full length sAPP and sAPP-derived peptides (250 nM each) were bath applied (dissolved in external medium described above) using a separate gravity driven application inlet. Recordings were done in whole-cell voltage clamp configuration at −70 mV with a double EPC-10 amplifier (HEKA Elektronik) under control of Patchmaster v2x32 software (HEKA Elektronik). Currents were low-pass filtered at 3 kHz and stored at 20 kHz. Patch pipettes were pulled from borosilicate glass using a multi-step puller (P-1000; Sutter Instruments). Pipette resistance ranged from 3 to 5 MΩ and was compensated to 75-80%. Only cells with series resistances <15 MΩ were included in analysis. All recordings were done at room temperature. Spontaneous events were detected using Mini Analysis program (Synaptosoft). mEPSCs and mIPSCs were separated on the basis of their distinct decay kinetics, using a threshold of 5 ms (*35*). This separation method accurately discriminates between mISPCs and mEPSC in paired recordings of minimal networks containing one GABAergic and one glutamatergic neuron: bicuculline (40 µM) blocked events with decay times above 5 ms, while CNQX (10 µM) blocked events with decay times below 5 ms. The mis-sorting error of mIPSCs and mEPSC using this method was determined to be 6.5% for mEPSCs and 3.5% for mIPSCs. Baseline was determined from an average of 60 sec of recordings prior to protein or drug treatment. Effect of treatment was determined from an average of 30 sec recordings after 140 sec of protein or drug treatment.

FM1-43 dye labeling

The experiments were performed in mature (15 - 28 days *in vitro*) cultures. Hippocampal neurons were imaged using a FV1000 spectral Olympus confocal microscope using a 60 × 1.2 NA water-immersion objective. The experiments were conducted at room temperature in extracellular Tyrode solution containing (in mM): NaCl, 145; KCl, 3; glucose, 15; HEPES, 10; $MgCl_2$, 1.2; $CaCl_2$, 1.2; pH adjusted to 7.4 with NaOH. For FM-based imaging and analysis, FM1-43 (10 μM) styryl dye was used to estimate basal synaptic vesicle recycling using a previously described protocol (*64*). Briefly, action potentials were elicited by passing 50 mA constant current for 1 ms through two platinum wires, separated by ~7 mm and close to the surface of the coverslip. The extracellular medium contained non-selective blocker of glutamate receptors (0.5 mM kynurenic acid) to block recurrent neuronal activity. 30 stimuli at 1 Hz were applied during FM1-43 loading, while 800 stimuli at 2 Hz during unloading. The fluorescence of individual synapses was determined from the difference between images obtained after staining and after destaining (ΔF). Detection of signals was done using custom-written scripts in MATLAB (Mathworks) as described before (*64*).

Slice preparation and electrophysiology

On the day of recording the brain of a 2-month-old Balb/c male mouse was quickly removed and 400 μm-thick horizontal slices were prepared in an ice-cold oxygenated buffer containing (in mM): sucrose, 182; KCl, 2.5; $MgSO_4$, 2; NaH_2PO_4, 1.25; $NaHCO_3$, 25; $CaCl_2$, 0.8; $MgCl_2$, 5; glucose, 25; ascorbate, 1; HEPES, 20. The slicing procedure was performed using a Leica VT1200 vibrating microtome. Slices were then transferred to a submerged recovery chamber at room temperature containing oxygenated (95% O2 and 5% CO2) storage artificial cerebrospinal fluid (ACSF) for 30min before the incubations (see below). The storage ACSF contained, in mM: NaCl, 100; KCl, 2.5; $MgSO_4$, 2; NaH_2PO_4, 1.25; $NaHCO_3$, 25; $CaCl_2$, 1.2; $MgCl_2$, 3; glucose, 20; ascorbate, 1; sodium pyruvate, 3 and HEPES, 20. The slices were incubated in the incubation chambers perfused with oxygenated storage ACSF containing the experimental agents for 90 min before performing field recordings: In the incubation chamber, control slices were perfused with normal storage ACSF while sAPPα slices were perfused with storage ACSF containing 1 μM sAPPα. CGP slices were perfused with storage ACSF containing 10 μM CGP54626 (Tocris). CGP + sAPPα slices were pre-

incubated in the chamber perfused with ACSF + CGP before being transferred into the chamber perfused with storage ACSF implemented with 10 μM CGP54626 + 1 μM sAPPα.

All recordings were performed as described previously (*64*) at 32-33°C in a recording chamber perfused with ACSF (4ml/min) on the stage of an Olympus BX51WI microscope equipped with IR optics and oblique illumination. Recording ACSF contains, in mM: NaCl, 129; KCl, 2.5; $CaCl_2$, 1.2; $MgCl_2$, 1.2; $NaHCO_3$, 25; NaH_2PO_4, 1.25; glucose, 15. Stimulation of the Schaffer collateral was delivered through a glass suction electrode (10 – 20 μm tip) filled with ACSF. fEPSPs were recorded using a glass pipette containing ACSF (1–2 MΩ) from proximal synapses in the CA1 stratum radiatum. Field recording experiments were analyzed using Clampfit.

Synthetic peptides

The following peptides were synthesized by Insight Biotechnology at >98% purity:

APP 17mer (204-220AA of APP695): acetyl-DDSDVWWGGADTDYADG-amide

Scrambled 17mer: acetyl-DWGADTVSGDGYDAWDD-amide

APP 9mer (204-212AA of APP695): acetyl-DDSDVWWGG-amide

APP10mer (211-220AA of APP695): acetyl-GGADTDYADG-amide

Nuclear Magnetic Resonance Spectroscopy

All NMR experiments were performed at 298 K on a Bruker Avance III HD 800 MHz spectrometer equipped with a TCI cryoprobe. For protein-based experiments, the sample contained 1mM U-[^{13}C, ^{15}N] labeled Sushi1 domain of $GABA_BR1a$ and 3mM unlabeled, natural-abundance APP 9mer peptide in 50 mM KP_i 50 mM NaCl pH 6.0 and 10 % D_2O for the lock. The NMR data were processed in TopSpin 3.5 (Bruker) or NMRPipe (*65*) and analyzed in CCPN (*66*). Nearly complete, unambiguous ^{1}H, ^{13}C and ^{15}N resonance assignments of the protein nuclei were obtained from a suite of standard multidimensional NMR experiments: 2D [^{1}H,^{15}N]-HSQC, [^{1}H,^{13}C]-HSQC, and constant-time

[^{1}H,^{13}C]-HSQC for the aromatic region; triple-resonance HNCACB, HN(CO)CACB, HNCO, HN(CA)CO, HBHA(CO)NH, C(CO)NH, and H(C)CH-TOCSY experiments; 2D (HB)CB(CGCD)HD and (HB)CB(CGCDCE)HE spectra for the aromatic resonances; and 3D ^{15}N-edited NOESY-HSQC and ^{13}C-edited NOESY-HSQC for aliphatics and aromatics. The resonance assignments were deposited in the BMRB data bank under the accession number 27581.

The 3D ^{15}N-edited NOESY-HSQC and ^{13}C-edited NOESY-HSQC spectra for aliphatics and aromatics, all acquired with the mixing time of 120 ms, were subsequently used for the protein structure calculation. The NOE cross-peaks, determined with CCPN Analysis (*66*), were combined with the dihedral angle restraints, obtained with DANGLE (*67*), and used as an input for the automated NOE assignment and structure calculations in CYANA v. 3 (*68*), followed by the final explicit solvent refinement in CNS (*69*). The 20 lowest-energy structures were retained and deposited in the PDB bank under the accession code 6HKC. The NMR structure calculation and refinement statistics are presented in Table S2.

For the peptide-based NMR experiments, we prepared the U-[^{13}C, ^{15}N] labeled version of the APP 9mer peptide (see above). The NMR samples contained either 0.1 mM U-[^{13}C, ^{15}N] labeled peptide alone or 0.35 mM U-[^{13}C, ^{15}N] labeled peptide and 2 molar equivalents of the unlabeled, natural abundance Sushi1 domain of GABA$_{B}$R1a in 50 mM KP_i 50 mM NaCl pH 6.0 and 10 % D_2O for the lock. The ^{1}H, ^{13}C and ^{15}N resonance assignments of the free peptide were obtained from 2D [^{1}H,^{15}N]-HSQC, [^{1}H,^{13}C]-HSQC, and constant-time [^{1}H,^{13}C]-HSQC spectra for the aromatic region; the ^{1}H-^{13}C planes of triple-resonance HNCACB, HNCO, and HBHA(CO)NH experiments; and 2D [^{1}H,^{15}N] HSQC-TOCSY, [^{1}H,^{13}C] HSQC-TOCSY, and 2D (HB)CB(CGCD)HD spectra. The obtained resonance assignments were transferred to the spectra of the protein-bound peptide and verified using a combination of the above experiments.

Upon binding to the protein, the U-[^{13}C, ^{15}N] peptide undergoes distinct spectral changes, including large chemical shift perturbations with a concomitant, substantial signal broadening. These indicate that the binding occurs in the intermediate exchange regime on the NMR timescale, which is consistent with the binding constant of 2.3 µM for the Sushi1 – APP 9mer complex (Fig. 5C) and could explain the absence of direct ^{1}H-^{1}H NOEs between the protein and the bound peptide. As typically seen for protein-peptide complexes with the binding constants in the 1 mM – 10 nM range (*70*), we detected a number of intermolecular NOEs transferred from the Sushi1 domain to the nuclei of the free peptide. These transferred NOEs (trNOEs) were observed in the [^{13}C, ^{15}N]-half-filtered, ^{13}C-edited 3D NOESY-

HSQC spectrum, recorded with the mixing time of 120 ms on the sample of U-[^{13}C, ^{15}N] labeled protein with the unlabeled peptide. The same experiment was repeated in 100% D_2O-based buffer to exclude the cross-peaks arising from the NOE transfer to non-C,N bound protein protons (e.g. OH groups of Ser, Thr, and Tyr residues).

The observed trNOEs allowed defining a set of 29 intermolecular distance restraints (Table S3), which were used to calculate the structure of the protein-peptide complex. The calculations were performed in Xplor-NIH (*71*), starting from the NMR structure of the Sushi1 domain obtained in this work and driven by the combination of the original, intramolecular protein-protein restraints and the trNOE-derived, intermolecular, protein-peptide contacts. With less than 2 unambiguous intermolecular distance restraints per peptide residue, this set was insufficient to accurately define the binding mode of the APP 9mer, as multiple conformers of the peptide could account for the observed NOEs. Nevertheless, the obtained structural model is consistent in that all solutions show the APP 9mer binding within the same pocket of Sushi1, where the Val and one of the Trp residues of the peptide make intimate contacts with the protein groups. The structural statistics for the complex of the Sushi1 domain of GABA$_B$R1a and the APP 9mer peptide are presented in Table S4, while its lowest-energy structure is shown in the main-text Fig. 5E.

In vivo 2-photon calcium imaging

Thy1-GCaMP6s mice (C57BL/6J-Tg(Thy1-GCaMP6s)GP4.12Dkim/J; JAX stock 025776) (*72*) (2-3 months old) were placed on a warming plate and anesthetized with isoflurane and respiration closely monitored for all surgical and experimental procedures. At least four days prior to the experiment, the hair, skin, and muscles on top of the skull were removed and a headplate and imaging chamber were affixed to the skull with cement. Mice were given 0.2 mg/kg buprenorphine (pain killer) and 15 mg/kg cefazolin (antibiotic) by I.P. injection every twelve hours for three days. On the night before and morning of the experiment mice were given 3.2 mg/kg dexamathosone (to prevent brain swelling). On the day of the experiment, a 1 mm craniotomy was performed at 2.3 mm posterior from bregma, 2 mm lateral from midline. The dura and pia overlying the cortical surface was removed and the cortex aspirated using a 27-gauge needle connected to a vacuum pump. Using a 16-gauge needle, the top fibers of the corpus callosum were carefully removed while sparing the bottom layer of fibers.

Using a peristaltic pump system, the imaging chamber was perfused with aCSF (150 mM NaCl, 5 mM KCl, 10 mM Glucose, 2 mM NaH_2PO_4, 2.5 mM $CaCl_2$, 1 mM $MgCl_2$, 10 mM HEPES, pH 7.4) at a flow-rate of approximately 1mL/minute. Baseline two-photon in vivo imaging (3-6 minutes in length depending on stability of image) were performed with aCSF perfusion alone. Then, 5 µM synthetic peptide (either APP 17mer or scrambled control 17mer) in aCSF was perfused for 60-90 mins and recordings were repeated. Baclofen (30 µM) in aCSF was applied for 15 mins before imaging. To wash out peptide, aCSF was perfused for 2 hours and recordings were then repeated.

The increased concentration of APP 17mer (5 µM) used for in vivo calcium imaging and the difference in concentration required for maximal effects in the different functional assays could be due to a number of technical reasons, including sensitivity of the assay, protein loss through the perfusion system, and efficiency of the protein to penetrate the tissue, in the case of experiments using acute hippocampal slices or superfusion of the exposed hippocampal CA1 region in vivo (particularly since a small layer of corpus callosum was needed to remain intact over the hippocampus to reduce damage to the underlying hippocampus).

A commercial two-photon microscope (Thorlabs Multiphoton Microscope, B-Scope) was used to record the calcium signal from the cell bodies of neurons in the pyramidal layer of dorsal CA1. Images were captured through a 16x objective (Nikon 16x, 0.8 NA), at a rate of 60Hz and consisting of 100x100µm squares sampled at 256x256 pixels. GCaMP6s was excited with a laser at a wavelength of 920nm (Mai Tai DeepSee, Spectra Physics). The maximum laser power at the objective was limited to 50 - 200 mW depending on the quality of the preparation. The microscope was controlled and the data was acquired using ScanImage 4.2. (*73*). Correction of brain motion artifacts, segmentation of neuronal cell bodies and extraction of neuronal signal was performed in Python (Python Software Foundation, Wilmington, DE), using the Calcium Imaging Analysis toolbox (CAIMAN). Additional analysis was performed in MATLAB (The Mathworks, Natick, MA). Calcium transients were initially automatically detected based on changes in fluorescent amplitude ($\Delta F/F$ at least five times higher than the baseline standard deviation) and later manually validated.

Statistical analysis

PRISM (Graphpad Software) was used to perform Student's t-test and analysis of variance (ANOVA), as appropriate and noted in figure legends. Bonferroni's, Dunnett's, or Tukey's *post hoc* analysis, as appropriate and noted in figure legends, was used to control for multiple comparisons. Sample sizes used for statistical analysis are noted in figure legends. (*$P < 0.05$; ** $P < 0.01$; ***$P < 0.001$).

5

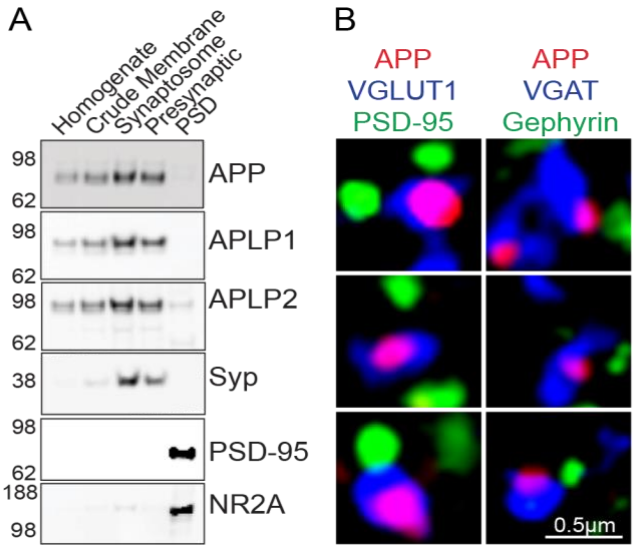

Fig. S1. Predominantly presynaptic localization of APP.

(A) Immunoblot of rat brain fractionations probed for APP family members and pre- (synaptophysin (Syp)) or post- (PSD-95 and NR2A) synaptic markers. **(B)** Structured Illumination Microscopy of mouse hippocampal sections immunostained for APP with presynaptic (VGLUT1 – excitatory; VGAT - inhibitory) and postsynaptic (PSD-95 – excitatory; Gephyrin - inhibitory) markers. Scale bar 0.5 µm.

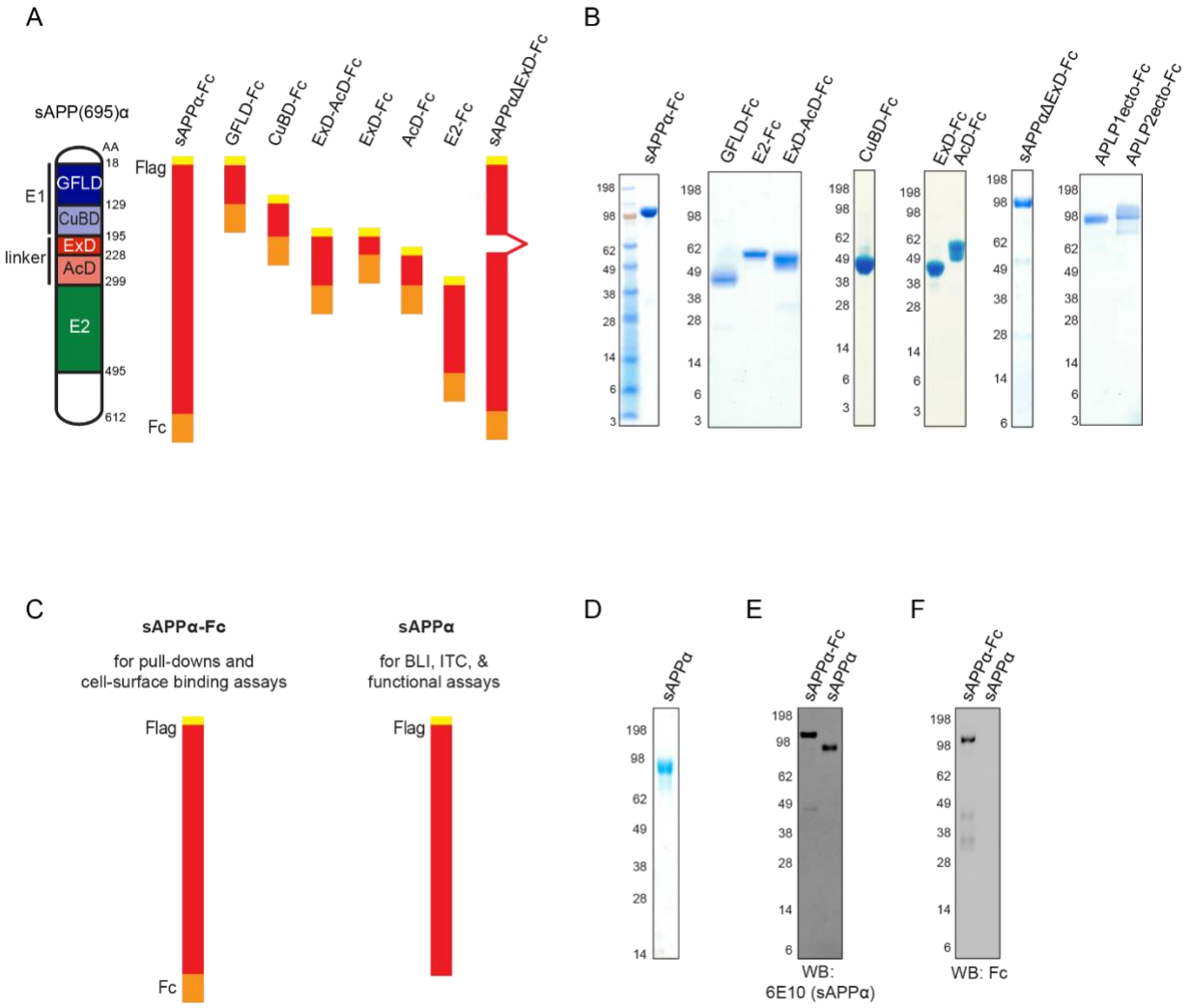

Fig. S2. Expression and biochemical characterization of purified proteins.

(A) Cartoon depicting C-terminally Fc-tagged purified proteins generated for pull-downs and cell-surface binding assays. **(B)** Coomassie stains of Fc proteins (used for cell-surface binding assays) expressed in HEK293T cells and purified by affinity chromatography. **(C)** Cartoon depicting sAPPα-Fc and sAPPα (Fc-tag enzymatically removed) used in functional assays. **(D)** Coomassie stain of purified sAPPα protein (used for functional assays) following cleavage of Fc tag. **(E)** Western blot of sAPPα-Fc and sAPPα purified proteins for 6E10 which recognizes the very C-terminal end of sAPPα. **(F)** Western blot of sAPPα-Fc and sAPPα purified proteins for the Fc-tag.

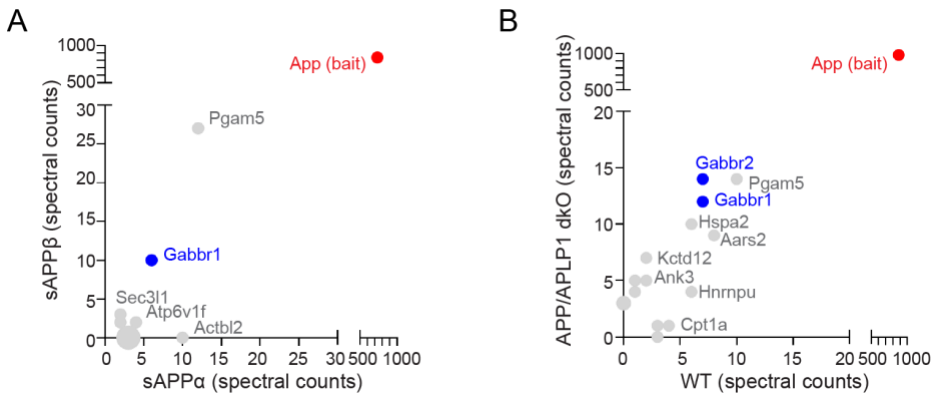

Fig. S3. Proteomics screen for synaptic interactors of sAPP*α*.

(A) Spectral counts of proteins identified by mass spectrometry from sAPPα-Fc and sAPPβ-Fc pull-downs performed in parallel on rat synaptosome extracts. **(B)** Spectral counts of proteins identified by mass spectrometry from sAPPα-Fc pull-downs performed in parallel on either wild type or *App*/*Aplp*1 dKO mouse synaptosome extracts. Only proteins which were absent in the Fc controls and present with > 2 spectral counts in a single trial are included. Cell-surface proteins are highlighted in blue.

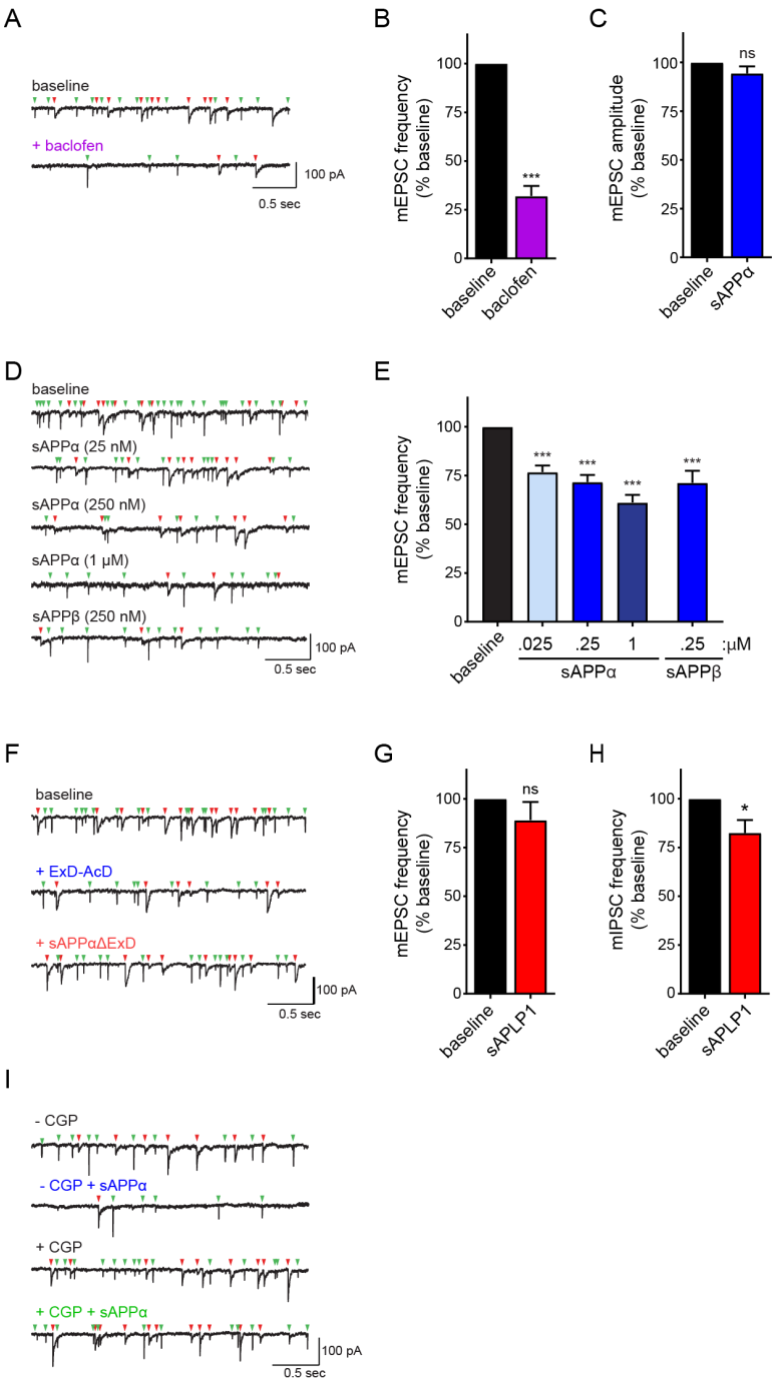

Fig. S4. Additional mPSC traces and experiments in primary hippocampal neurons.

(A,B) Example traces of mEPSCs (green arrowheads) and mIPSCs (red arrowheads) (A) and average mEPSC frequency normalized to baseline (B) recorded from primary hippocampal neurons cultured from wild type mouse

before (baseline) and after treatment with baclofen, a GABA$_B$R agonist (30 µM, n=12 cells, N=2, paired t-test). **(C)** Average mEPSC amplitude normalized to baseline recorded from primary neurons before (baseline) and after treatment with sAPPα (250 nM, n=13, N = 3, paired t-test). **(D,E)** Example traces of mEPSCs (green arrowheads) and mIPSCs (red arrowheads) (D) and average mEPSC frequency normalized to baseline (E) recorded from primary neurons before (baseline) and after treatment with 25 nM, 250 nM, or 1 µM of sAPPα or 250 nM sAPPβ. (n= 16-20, N=3) (one way ANOVA with Dunnett's *post hoc* analysis). The concentrations of APP peptides applied in our experiments are likely within the physiological range, since a high concentration of APP (42 µM) at the synapse has been reported (*25*) and the apparent binding affinity between APP and GABA$_B$R1a is 400-800nM (Fig 1G), an affinity well within the range of known synaptic interactions (*74*, *75*). **(F)** Example traces of mEPSCs (green arrowheads) and mIPSCs (red arrowheads) recorded from primary neurons before (baseline) and after treatment with either ExD-AcD or sAPPαΔExD. **(G)** Average mEPSC frequency normalized to baseline recorded from wild type neurons before (baseline) and after treatment with sAPLP1 (n=17, N=3, t-test). **H)** Average mIPSC frequency normalized to baseline recorded from wild type neurons before (baseline) and after treatment with sAPLP1 (n=17, N=3, t-test). **(I)** Example traces of mEPSCs (green arrowheads) and mIPSCs (red arrowheads) recorded from primary neurons before (baseline) and after treatment with sAPPα either without (blue) or with (green) preincubation with CGP55845 (CGP, 5 µM), a GABA$_B$R antagonist. Means ± SEM. The number of neurons is defined by n. The number of independent experiments is defined by N. * $P < 0.05$; ***$P < 0.001$.

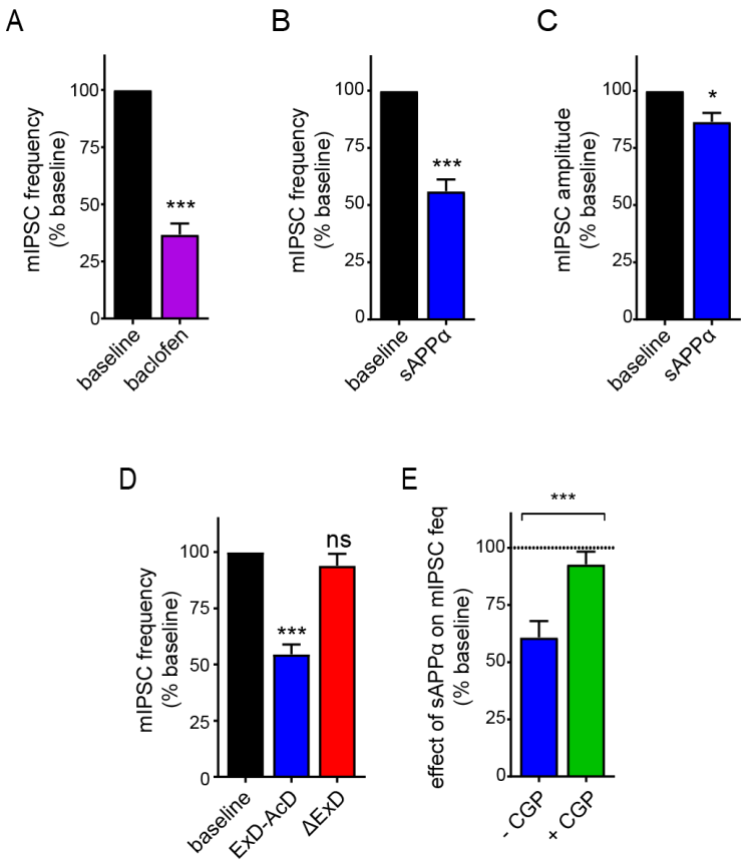

Fig. S5. sAPPα reduces mIPSC frequency via GABAʙR1a in cultured hippocampal neurons.

(A) Average mIPSC frequency normalized to baseline recorded from primary hippocampal wild type neurons before (baseline) and after treatment with baclofen, a GABAʙR agonist (30 µM, n=12 cells, N = 2 paired t-test). **(B,C)** Average mIPSC frequency (B) and amplitude (C) normalized to baseline recorded from primary neurons before (baseline) and after treatment with sAPPα (250 nM, n=13 cells from 3 independent experiments, paired t-test). **(D)** Average mIPSC frequency normalized to baseline recorded from primary neurons before (baseline) and after treatment with either sAPPα ExD-AcD or sAPPαΔExD (n=17-20, N=3, one way ANOVA with Dunnett's *post hoc* analysis). **(E)** Quantification of the effect of sAPP on mIPSC frequency normalized to baseline either without or with preincubation with CGP55845 (5 µM, CGP), a GABAʙR antagonist. Dotted line denotes baseline (n=14-17, N=3, unpaired t-test). Means ± SEM. The number of neurons is defined by n. The number of independent experiments is defined by N. * P < 0.05; *** P < 0.001.

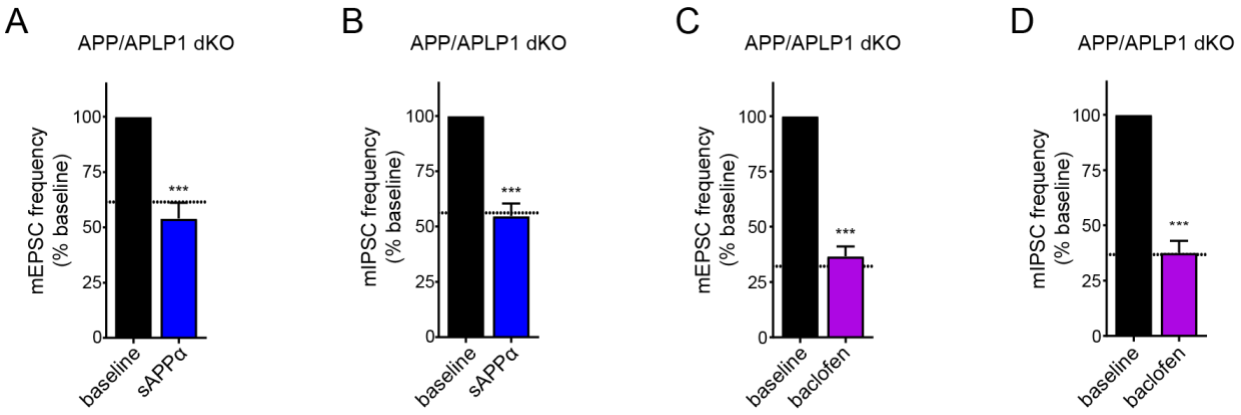

Fig. S6. Both sAPPα and baclofen have similar effects in *App*/*Aplp1* dKO neurons as in wild type neurons.

(A,B) Average mEPSC (A) and mIPSC (B) frequency normalized to baseline recorded from *App*/*Aplp1* dKO primary hippocampal neurons before (baseline) and after treatment with 250nM sAPPα (n=11, N=3, paired t-test). Dotted line denotes effect in wild type neurons. **(A,B)** Average mEPSC (A) and mIPSC (B) frequency normalized to baseline recorded from *App*/*Aplp1* dKO primary hippocampal neurons before (baseline) and after treatment with 30 µM baclofen (n=14, N=3, paired t-test). Dotted line denotes effect in wild type neurons. Means ± SEM. The number of neurons is defined by n. The number of independent experiments is defined by N. $P < 0.001$.

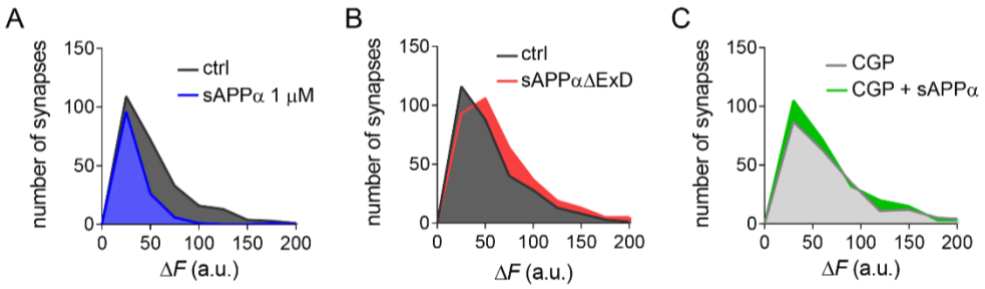

Fig. S7. Plots of change in fluorescence intensity (ΔF) of FM1-43 signals at individual boutons of cultured hippocampal neurons.

(A) Δ*F* histograms before (ctrl) and after 1μM sAPPα application from a representative experiment. **(B)** Δ*F* histograms before (ctrl) and after 1μM sAPPαΔExD application from a representative experiment. **(C)** ΔF histograms before and after application of 1 μM sAPPα in the presence of a GABA$_B$R antagonist, CGP54626 (CGP) from a representative experiment.

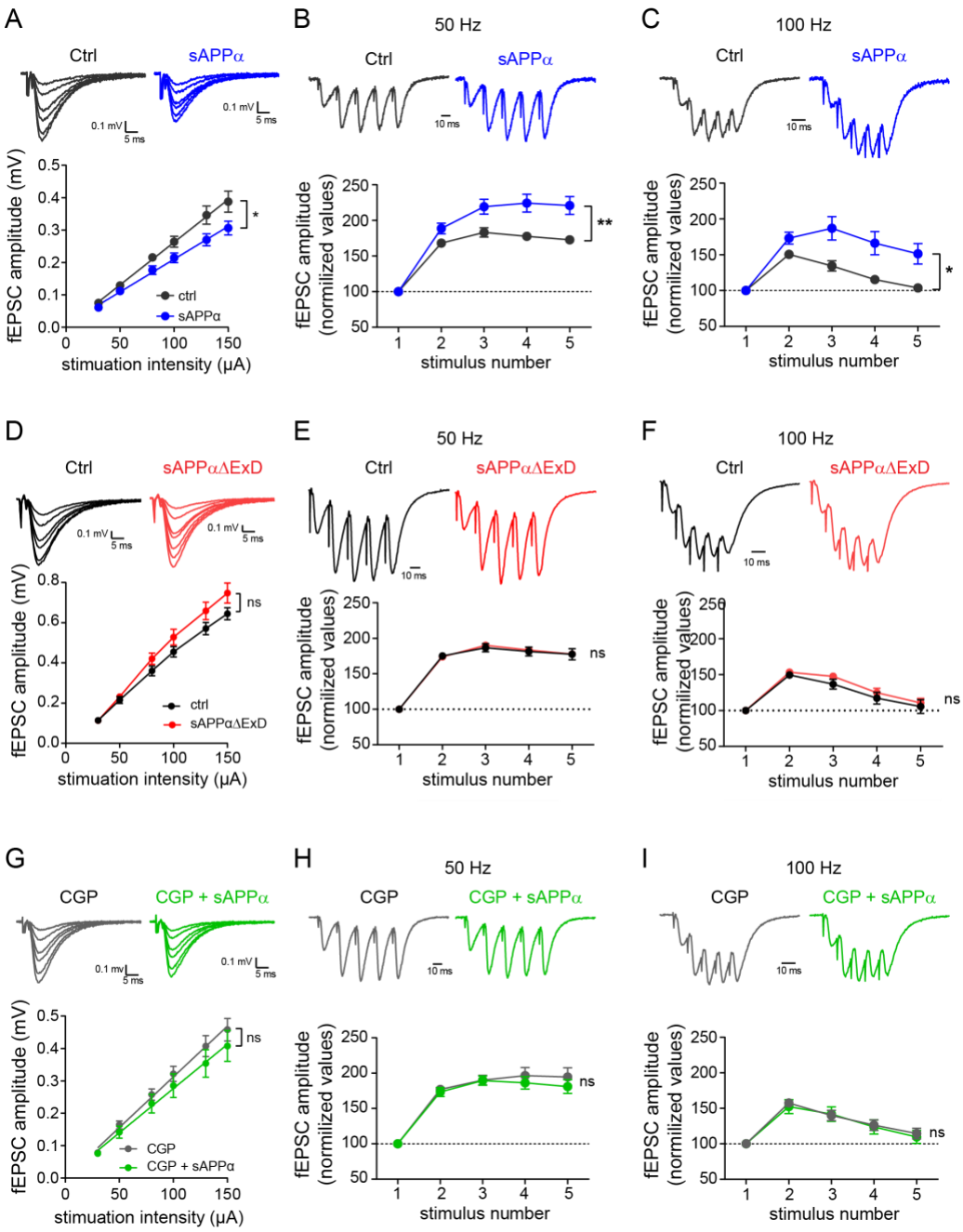

Fig. S8. sAPPα reduces basal synaptic transmission and increases short-term plasticity via GABAʙR1a at Schaffer collateral synapses.

(A) Representative traces of fEPSPs (upper) and input-output curves (lower) recorded at Schaffer collaterals (SCs) from hippocampal slices incubated without (black, control (ctrl)) or with sAPPα (blue) (ctrl, n=9, N=7; sAPPα, n=12,

N=7). **(B,C)** Representative traces (upper) and average fEPSP amplitude (lower) in response to high-frequency burst stimulation at 50 Hz (B) and 100 Hz (C) (for each frequency: n = 10, N = 7 for Ctrl; n = 12, N = 7 for sAPPα) in slices incubated without (black) or with sAPPα (blue). fEPSPs were normalized to the peak amplitude of the first response. **(D)** Representative traces of fEPSPs (upper) and input-output curves (lower) recorded at SCs from hippocampal slices incubated without (black) or with 1 µM sAPPαΔExD (red) (Ctrl, n=10, N=4; sAPPα -ΔExD, n=9, N=4). **(E,F)** Representative traces (upper) and average fEPSP amplitude (lower) in response to high-frequency burst stimulation at 50 Hz (J) and 100 Hz (K) (for each frequency: n = 10, N = 4 for Ctrl; n = 9, N = 4 for sAPPαΔExD) in slices incubated without (black) or with sAPPαΔExD (red). **(G)** Representative traces of fEPSPs (upper) and input-output curves (lower) recorded from hippocampal slices incubated with CGP 54626 (CGP) alone (grey) and slices incubated with CGP + sAPPα (green). (CGP, n=9, N=4; CGP + sAPPα, n=8, N=4). **(H,I)** Representative traces (upper) and average fEPSP amplitude (lower) in response to high-frequency burst stimulation at 50 Hz (F) and 100 Hz (G) (for each frequency: n = 9, N =4 for CGP; n = 8, N = 4 for CGP + sAPPα) from slices incubated with CGP alone (grey) or with CGP + sAPPα (green). fEPSPs were normalized to the peak amplitude of the first response. Means ± SEM. The number of slices is defined by n, the number of mice by N. Two-way ANOVA analysis; * $P < 0.05$; ** $P < 0.01$; *** $P < 0.001$.

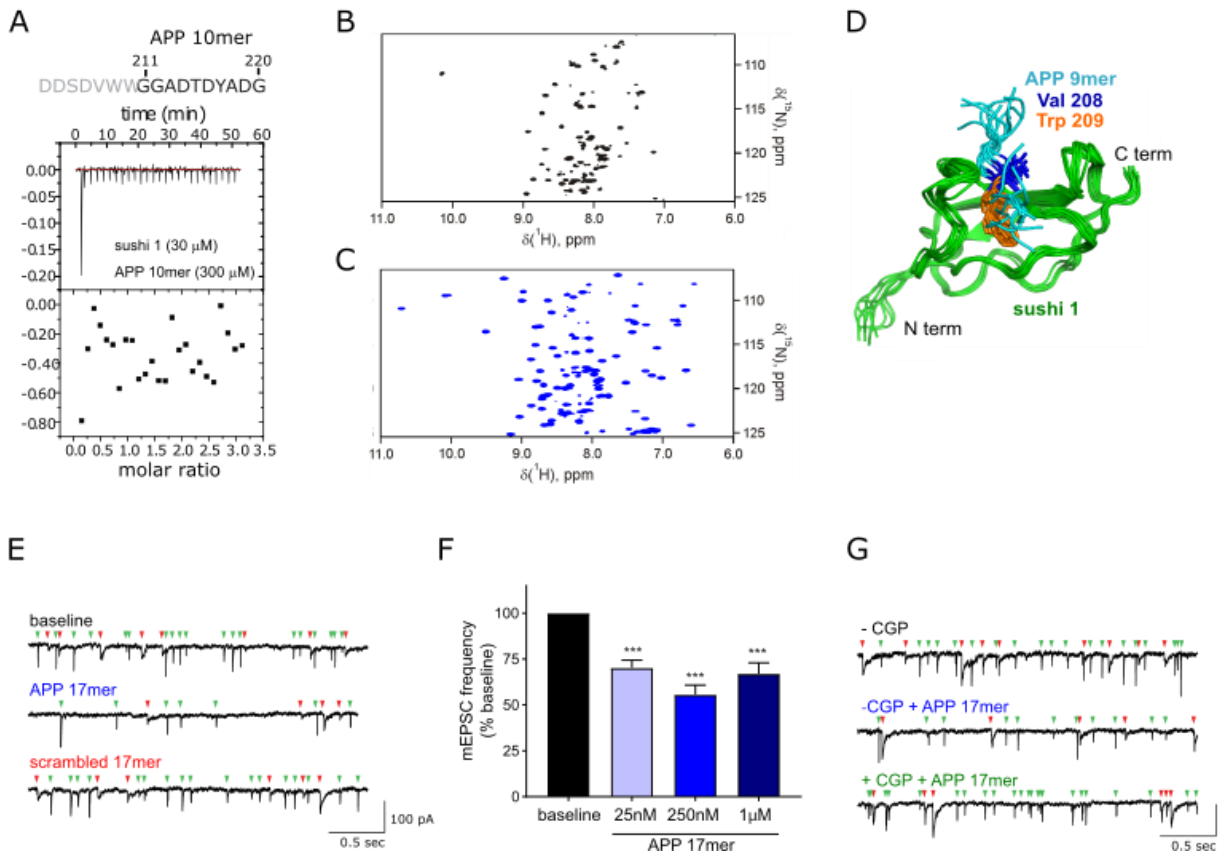

Fig. S9. A short peptide within the APP ExD suppresses synaptic vesicle release via GABA$_B$R1a.

(A) ITC binding experiment of purified sushi 1 and synthetic APP 10mer peptide corresponding to 211-220AA within the ExD of APP695. **(B,C)** The [^{1}H,^{15}N] HSQC spectra of the U-[^{13}C, ^{15}N] labeled sushi 1 domain of GABA$_B$R1a alone (B) or in the presence of 3 molar equivalents of the APP 9mer peptide (C). As reported before (*76*), the poor signal dispersion, low spectral resolution, and a small number of resonances in (B) indicate a high degree of structural disorder of the isolated sushi 1 domain. Addition of the APP 9mer peptide stabilizes the sushi 1 domain, as evidenced by a drastic spectral improvement seen in (C). **(D)** An ensemble of 10 lowest-energy structures of the complex between sushi 1 domain of GABA$_B$R1a (green) and the APP 9mer peptide (cyan). The Val 5 and Trp 6 residues of the APP 9mer peptide (Val 208, Trp 209 of APP695) are shown as sticks and colored blue and orange, respectively. **(E)** Example traces of mEPSCs (green arrowheads) and mIPSCs (red arrowheads) recorded from primary neurons before (baseline) and after treatment with synthetic 17mer APP peptide (250 nM, APP695 204-220AA) or scrambled 17mer

control peptide. **(F)** Average mEPSC frequency normalized to baseline recorded from primary neurons before (baseline) and after treatment with 25 nM, 250 nM, or 1 µM of APP 17mer (n = 15-16 cells, N = 6 experiments) (one way ANOVA with Dunnett's *post hoc* analysis). **(G)** Example traces of mEPSCs (green arrowheads) and mIPSCs (red arrowheads) recorded from primary neurons before (baseline) and after treatment with 250 nM synthetic 17mer APP peptide (APP695 204-220AA) either without (blue) or with (green) preincubation with CGP55845 (CGP, 5 µM), a $GABA_BR$ antagonist.

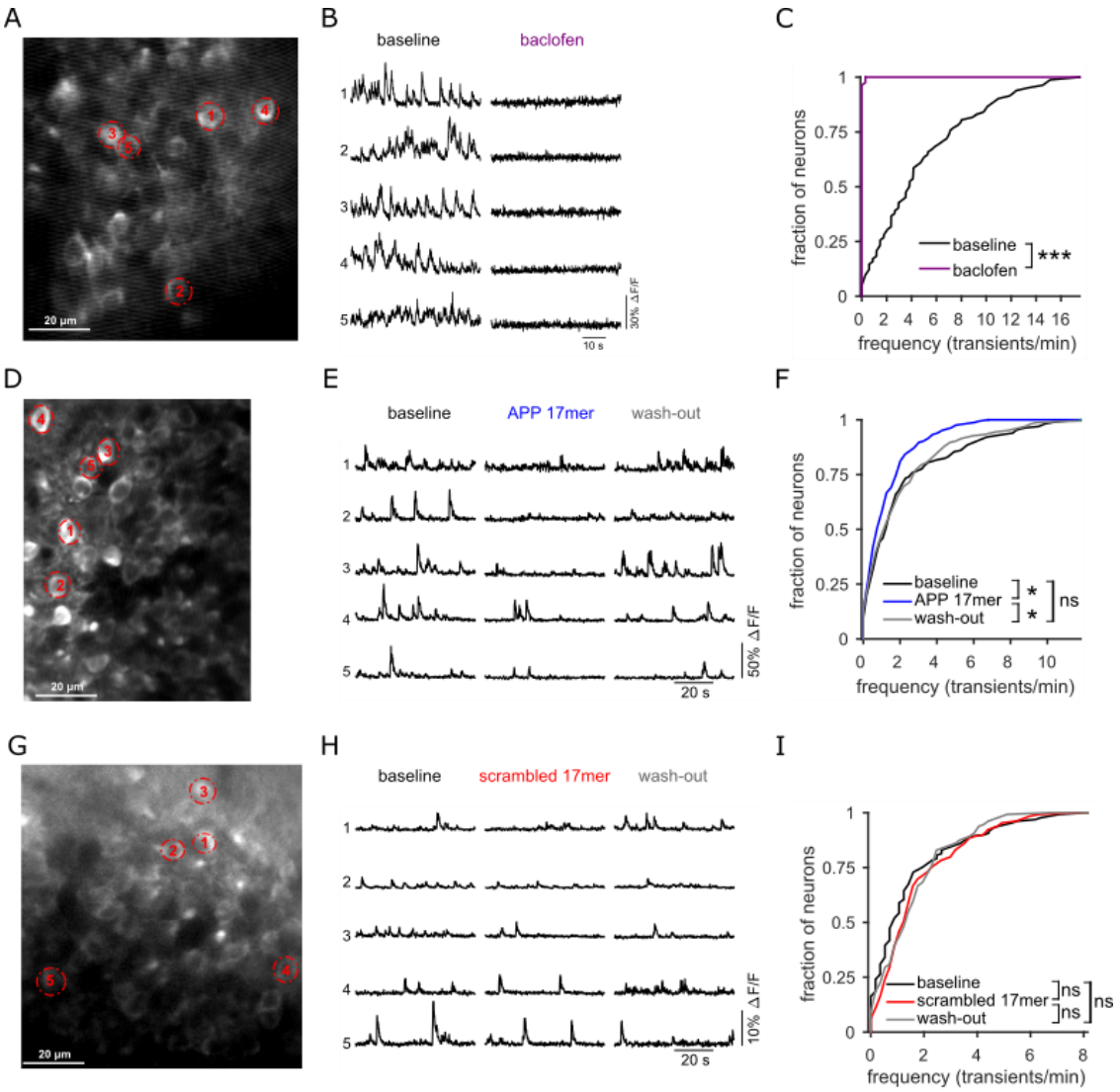

Fig. S10. A 17AA peptide corresponding to the GABA$_B$R1a binding region within APP suppresses neuronal activity *in vivo*.

(A) *in vivo* image of CA1 hippocampal neurons of Thy1-GCaMP6s mice. **(B)** Calcium traces of five representative neurons, labeled in panel A, before (baseline) and during bath application of 30 µM baclofen. **(C)** Cumulative distribution of the frequency of calcium transients at baseline (blue line) and during baclofen bath application (red line) (n=82 neurons from 3 mice). **(D)** *in vivo* image of CA1 hippocampal neurons of Thy1-GCaMP6s mice. **(E)** Calcium traces of five representative neurons, labeled in panel A, before (baseline), during bath application of 5 µM

APP 17mer peptide corresponding to the GABA$_B$R1a binding region within APP (APP 17mer), and following wash-out. **(F)** Cumulative distribution of the frequency of calcium transients at baseline (blue line), during APP 17mer bath application (red line), and after wash-out (grey line) (n=165 neurons from 1 mouse). **(G)** *in vivo* image of CA1 hippocampal neurons of Thy1-GCaMP6s mice. **(H)** Calcium traces of five representative neurons, labeled in panel A, before (baseline), during bath application of 5 µM scrambled 17mer control peptide, and following wash-out. **(I)** Cumulative distribution of the frequency of calcium transients at baseline, during scrambled 17mer bath application (red line), and after wash-out (grey line) (n=129 neurons from 2 mice). Wilcoxon rank sum test. * $P \leq 0.05$, *** $P \leq 0.001$; NS $P>0.05$

Trial:		1		2		3		4		5	
Figure:		1B (X-axis)		1B (Y-axis) S3A (X-axis)		S3A (Y-axis)		S3B (X-axis)		S3B (Y-axis)	
Independent Experiment:		1		2				3			
Synaptosomes:		rat		rat				mouse			
								WT		APP/APLP1 dKO	
Bait:		sAPPα-Fc		sAPPα-Fc		sAPPβ-Fc		sAPPα-Fc			
Description	**Gene Name**	**spectra**	**peptide**	**spectra**	**peptide**	**spectra**	**peptide**	**spectra**	**peptide**	**spectra**	**peptide**
Cell-Surface Proteins											
Amyloid beta A4 protein	App	847	168	735	137	841	148	882	143	983	148
Gamma-aminobutyric acid (GABA) B receptor 1	Gabbr1	6	5	6	6	10	7	7	6	12	11
Gamma-aminobutyric acid type B receptor subunit 2	Gabbr2	3	3	-	-	-	-	7	7	14	12
Vesicle-associated membrane protein 3	Vamp3	4	4	-	-	-	-	-	-	-	-
Amyloid-like protein 2	Aplp2	4	3	-	-	-	-	-	-	-	-
Other Proteins											
Serine/threonine-protein phosphatase PGAM5, mitochondria	Pgam5	17	11	12	10	27	13	10	9	14	12
Beta-Actin-Like Protein 2	Actbl2	20	14	10	7	-	-	-	-	-	-
Heterogeneous nuclear ribonucleoprotein	Hnrnpu	11	11	2	2	2	2	6	6	4	4
Ankyrin-G	Ank3	10	8	3	3	-	-	2	2	5	5
Alanine--tRNA ligase, mitochondrial	Aars2	-	-	-	-	-	-	8	7	9	6
Heat shock-related 70 kDa protein 2	Hspa2	-	-	-	-	-	-	6	5	10	9
BTB/POZ domain-containing protein KCTD12	Kctd12	-	-	-	-	-	-	2	2	7	6
BTB/POZ domain-containing protein KCTD16	Kctd16	-	-	3	2	-	-	1	1	4	4
Guanine nucleotide binding protein beta 4	Gnb4	7	3	-	-	-	-	-	-	-	-
V-type proton ATPase subunit F	Atp6v1f	-	-	4	3	2	2	-	-	-	-
Erythrocyte Membrane Protein Band 4.9 (Dematin)	Epb49	6	6	-	-	-	-	-	-	-	-
Alpha-synuclein	Snca	-	-	-	-	-	-	1	1	5	5
SEC3-Like 1 (Exocyst Complex Component Sec3)	Sec3l1	-	-	2	2	3	3	-	-	-	-
F-actin-capping protein subunit alpha-2	Capza2	5	4	-	-	-	-	-	-	-	-
Carnitine O-palmitoyltransferase 1	Cpt1a	-	-	-	-	-	-	4	4	1	1
Acyl-CoA-binding protein	Dbi	4	4	-	-	-	-	-	-	-	-
Band 4.1-like protein 1	Epb41l1	4	4	-	-	-	-	-	-	-	-
Myosin phosphatase Rho-interacting protein	Mprip	4	4	-	-	-	-	-	-	-	-
Elongation factor 1-alpha 1	Eef1a1	-	-	-	-	-	-	3	3	1	1
ATP/GTP binding protein 1	Agtpbp1	-	-	3	3	-	-	-	-	-	-
Ras-related protein Rab-1B	Rab1b	-	-	3	3	-	-	-	-	-	-
SET Binding Factor 1	Sbf1	-	-	3	3	-	-	-	-	-	-
ATP-citrate synthase	Acly	3	3	-	-	-	-	-	-	-	-
Actin-Like Protein 3B	Actr3b	3	3	-	-	-	-	-	-	-	-
Rho guanine nucleotide exchange factor 11	Arhgef11	3	3	-	-	-	-	-	-	-	-
F-actin-capping protein subunit alpha-1	Capza1	3	3	-	-	-	-	-	-	-	-
Rab GDP dissociation inhibitor beta	Gdi2	3	3	-	-	-	-	-	-	-	-
Guanine nucleotide-binding protein G(i) subunit alpha-1	Gnai1	3	3	-	-	-	-	-	-	-	-
G Protein Regulated Inducer Of Neurite Outgrowth 1	Gprin1	3	3	-	-	-	-	-	-	-	-
Polyadenylate-binding protein 1	Pabpc1	3	3	-	-	-	-	-	-	-	-
THO complex subunit 4	Thoc4	3	3	-	-	-	-	-	-	-	-
Disco-interacting protein 2 homolog B	Dip2b	-	-	-	-	-	-	3	3	-	-
Copine-7	Cpne7	-	-	-	-	-	-	-	-	3	3

Table S1.

Mass Spectrometry Results for sAPP-Fc pull-down. A total of 5 pull-downs were performed over 3 independent experiments. The bait (sAPPα-Fc or sAPPβ-Fc) and source of synaptosome material (rat or mouse) is indicated. The corresponding graphs in Fig. 1B and S3A,B are indicated. Only proteins which were absent in the Fc controls and present with > 2 spectral counts in a single trial are included. There may be additional sAPP binding partner(s) with lower affinity that we were unable to capture under the relatively stringent conditions used in these screens.

Distance restraints	
Total	1641
Intra-residue (i - j = 0)	390
Sequential (|i - j| = 1)	477
Medium range (1 < |i - j| < 5)	233
Long range (|i - j| ≥ 5)	541
Dihedral angle restraints	
ϕ and ψ	112
Restraints violations	
NOE, > 0.5 Å	0
Dihedral angle, > 5°	2.8
RMSD from average,[a] Å	
Backbone	0.64 ± 0.10
Heavy atoms	1.04 ± 0.10
Ramachandran statistics,[b] %	
Most favored	62.1
Allowed	35.4
Additionally allowed	1.6
Disallowed	0.9

Table S2.

Structural statistics over the 20 lowest-energy, water-refined NMR structures of the sushi 1 domain of GABA$_B$R1$_a$ when bound to the APP 9mer peptide. [a] Calculated for residues 5-73 (the ordered region). [b] Calculated with PROCHECK-NMR.

Unambiguous		Ambiguous	
APP 9mer atom	sushi 1 atom	APP 9mer atom	sushi 1 atom
Ser 3 Hb1	Arg 19 Ha	Any of the Hd1, He3, Hz3, Hh2 atoms of Trp 6 or Trp 7	Ile 9 Hg2*
Asp 4 Hb*	Arg 21 Ha		Ile 9 Hd1*
Val 5 Hg1*	Gly 17 Ha1		Gly 16 Ha1
	Gly 17 Ha2		Gly 16 Ha2
	Val 43 Hb		Arg 19 Hg*
	Val 43 Hg1*		Val 28 Hg1*
	Val 43 Hg2*		Val 28 Hg2*
Val 5 Hg2*	Arg 19 Ha		Val 43 Hg1*
	Arg 19 Hb1		Val 43 Hg2*
	Arg 19 Hb2		Cys 44 Ha
	Arg 19 Hd1		Arg 45 Ha
	Arg 19 Hd2		Arg 45 Hg1
	Val 43 Hg1*		Arg 45 Hg2
Trp 6 Hb*	Ile 18 Hg2*		
	Val 28 Hg1*		
	Val 28 Hg2*		

Table S3.

Intermolecular distance restraints for the complex between the sushi 1 domain of $GABA_BR1_a$ and the APP 9mer peptide, derived from trNOEs and defined as the upper-limit bounds of 5 Å.

5

Intramolecular protein restraints	
NOE	1641
Dihedral angles	112
Intermolecular restraints	
unambiguous NOEs	16
ambiguous NOEs	13
Restraints violations	
protein NOE, > 0.5 Å	3.8
Dihedral angle, > 5°	10.3
intermolecular NOE, > 0.5 Å	0
RMSD from average, Å	
Backbone, protein[a]	0.42 ± 0.08
Heavy atoms, protein[a]	0.75 ± 0.09
Backbone, peptide	1.15 ± 0.33
Heavy atoms, peptide	1.92 ± 0.27
Backbone, VWW motif[b]	0.45 ± 0.07
Heavy atoms, VWW motif[b]	1.40 ± 0.25
Ramachandran statistics,[c] %	
Most favored	59.8
Allowed	36.7
Additionally allowed	3.0
Disallowed	0.5

Table S4.

Structural statistics over the 10 lowest-energy solutions for the complex of the sushi 1 domain of GABA$_B$R1$_a$ and the APP 9mer peptide. [a] Calculated for residues 5-73 (the ordered region) of the sushi 1 domain. [b] Calculated for residues Val 5, Trp 6, and Trp 7 of the APP 9mer peptide. [c] Calculated with PROCHECK-NMR.

Movie S1. *in vivo* imaging of CA1 hippocampal neurons of Thy1-GCaMP6s mice with application of APP 17mer peptide

Movie of *in vivo* 2-photon calcium imaging (left) and calcium traces (right) of the same five representative neurons as in Figure 4B,C before (top) and during (bottom) bath application of 5 µM APP 17mer peptide.

Movie S2. *in vivo* imaging of CA1 hippocampal neurons of Thy1-GCaMP6s mice with application of scrambled 17mer peptide

Movie of *in vivo* 2-photon calcium imaging (left) and calcium traces (right) of the same five representative neurons as in Figure 4E,F before (top) and during (bottom) bath application of 5 µM scrambled 17mer peptide.